# Hyperactivation of MEK1 in cortical glutamatergic neurons results in projection axon deficits and aberrant motor learning

*George R. Bjorklund[1,2], *Katherina P. Rees[1], Kavya Balasubramanian[1], Lauren T. Hewitt[1,3], Kenji Nishimura[1,4], Jason M. Newbern[1#]

[1]School of Life Sciences and [2]School of Biological and Health Systems Engineering, Arizona State University, Tempe, AZ, 85287

[3]Present address: Porter Neuroscience Center, Eunice Kennedy-Shriver National Institute of Child Health and Human Development, National Institutes of Health, Bethesda, Maryland, 20892

[4]Present address: Institute for Neuroscience, The University of Texas-Austin, Austin, Texas, 78712

*These authors contributed equally

[#]Corresponding author & ORCID ID# 0000-0003-2865-0112

***Keywords***

connectivity, cortex, development, RASopathy, kinase, axon

***Summary statement:***

MEK-ERK1/2 hyperactivation in developing cortical excitatory neurons is sufficient to decrease long-range axonal outgrowth, which coincides with reduced Arc expression and deficits in aspects of skilled motor learning by adulthood.

***Abstract***

Abnormal Extracellular Regulated Kinase 1/2 (ERK1/2) signaling is linked to multiple neurodevelopmental diseases, especially the RASopathies, which typically exhibit ERK1/2 hyperactivation in neurons and non-neuronal cells. To better understand how excitatory neuron-autonomous ERK1/2 activity regulates the development of the mouse motor cortex, we conditionally expressed a hyperactive MEK1$^{S217/221E}$ variant using *Nex/NeuroD6:Cre*. Our results show that MEK1$^{S217/221E}$ expression led to persistent hyperactivation of ERK1/2 in neocortical axons, but not excitatory neuron somas or nuclei. We noted reduced axonal arborization of multiple subcortical target domains in mutants and reduced cortical expression of the activity dependent gene, ARC. These changes did not coincide with significant differences in voluntary locomotor activity or motor performance in the accelerating rotarod task. However, motor learning in a single-pellet retrieval task was significantly diminished in *Nex/NeuroD6:Cre*; *MEK1$^{S217/221E}$* mutants. Restriction of MEK1$^{S217/221E}$ expression to layer V cortical neurons recapitulated axonal outgrowth deficits, however, had no effect on motor learning. Collectively, these results indicate that within the cortex, glutamatergic neuron-autonomous hyperactivation of MEK1 is sufficient to drive deficits in axon outgrowth, activity dependent gene expression, and skilled motor learning.

45 ***Introduction***

46 Many extracellular cues important for forebrain development, such as fibroblast growth
47 factors (FGFs) and neurotrophins, activate receptor tyrosine kinases (RTKs) to modulate a wide
48 range of cellular behaviors. Ligand-bound RTKs initiate intracellular signaling via numerous
49 kinase cascades, including the PI3K, PLC, PKC, and Extracellular Regulated Kinase 1/2 (ERK1/2)
50 pathways (Lemmon and Schlessinger, 2010). Activation of ERK1/2 downstream of RTK signaling
51 has been well-studied, which requires RAS-dependent activation of RAF isoforms and
52 subsequent phosphorylation of MEK1 and MEK2 at two conserved residues in the kinase domain,
53 $Ser^{218/222}$ and $Ser^{222/226}$, respectively (Klomp et al., 2021; Lavoie et al., 2020). Activated MEK1/2
54 then phosphorylates ERK1 and ERK2, which ultimately act upon hundreds of cytosolic and
55 nuclear substrates (Ünal et al., 2017). ERK1/2 signaling has frequently been linked to the control
56 of cell proliferation, differentiation, survival, synaptic plasticity, and learning (Atkins et al., 2001;
57 Gómez-Palacio-Schjetnan and Escobar, 2008; Jeanneteau et al., 2010; Kalil and Dent, 2014;
58 Mebratu and Tesfaigzi, 2009; Nowaczyk et al., 2014; Polleux and Snider, 2010; Thomas and
59 Huganir, 2004). However, this broad repertoire obscures the intricate, context-dependent
60 functions of ERK1/2 signaling that are highly contingent on the precise developmental stage, cell
61 type, and/or extracellular cue (Santini et al., 2019; Shaul and Seger, 2007). Developing neurons
62 in particular exhibit complex, subtype specific responses to modifications in ERK1/2 activity that
63 are not fully understood (Ryu and Lee, 2016).

64 Key regulators in the RTK-ERK1/2 signaling network are frequently mutated in a family of
65 developmental syndromes known collectively as the "RASopathies" (Jindal et al., 2015; Kim and
66 Baek, 2019; Rauen, 2013; Rauen, 2022). Well-defined mutations have been identified in
67 individual syndromes within the RASopathy superfamily, such as Noonan syndrome (NS),
68 Neurofibromatosis type 1 (NF1), Costello syndrome (CS), and Cardio-facio-cutaneous syndrome
69 (CFC). NS and NF1 are common RASopathies with a combined frequency of ~1:2000 births
70 (Rauen, 2013; Tidyman and Rauen, 2009). However, >50 distinct RASopathy mutations in over
71 10 different genes within the RTK-ERK1/2 network have been reported (Brown et al., 2012;

72 Gutmann et al., 2012; Jindal et al., 2015; Kaul et al., 2015; Rauen, 2022). Upstream RASopathy
73 mutations in NF1, SHP2, and RAS have been shown to modulate PI3K/Akt, PKC, and/or
74 Rho/ROCK activity, in addition to the ERK1/2 pathway (Anastasaki and Gutmann, 2014; Brown
75 et al., 2012; Castellano and Downward, 2011; Kaul et al., 2015). ERK1/2 hyperactivation is,
76 however, thought to be a core, common feature of nearly all RASopathies. Thus, pharmacological
77 inhibitors of ERK1/2 regulators have been an important focus for therapeutic development
78 (Guilding et al., 2007; López-Juárez et al., 2017; Nakamura et al., 2009; Wang et al., 2012; Wu
79 et al., 2011). ERK1/2 also represents a convergent target downstream of multiple genetic risk
80 factors for autism and is abnormally activated in models of Fragile X and 16p11.2 deletion
81 syndrome (Chung et al., 2021; Osterweil et al., 2013; Wen et al., 2016). Therefore, understanding
82 the cell-specific effects of ERK1/2 activity in the developing forebrain may shed light on potential
83 neuropathological processes in multiple developmental disorders (Bernardino et al., 2022; Li et
84 al., 2005; Roskoski, 2019).

85 MRI-based studies suggest that differences in both cortical structural and functional
86 connectivity are a critical aspect of intellectual disability and cognitive changes in RASopathies
87 and autism (Aydin et al., 2016; Chang et al., 2016; Fattah et al., 2021; Filippi et al., 2013; Ibrahim
88 et al., 2017; Owen et al., 2018; Tomson et al., 2015; Zamboni et al., 2007). Changes in motor
89 cortex function have been detected in RASopathies and individuals with Noonan Syndrome note
90 that treatments for cognitive and musculoskeletal abnormalities are a high priority (Bernardino et
91 al., 2022; Doherty et al., 2023; Tiemens et al., 2023). Yet, it is difficult to discern whether functional
92 changes are a result of aberrant signaling in neurons, myelinating oligodendrocytes, or complex
93 interactions during development. Studies have shown a specific role for ERK1/2 signaling in
94 regulating rodent myelinating glial development *in vivo* (Ishii et al., 2012; Ishii et al., 2013;
95 Newbern et al., 2011), and pharmacological MEK1/2 inhibition rescues myelination deficits
96 caused by RASopathic signaling in mature oligodendrocytes (López-Juárez et al., 2017; Mayes
97 et al., 2013). Effects of upstream RASopathy mutations in SynGAP1, NF1, and RAS that activate
98 multiple downstream cascades, selectively in neurons, have been explored (Clement et al., 2012;

99 Cui et al., 2008; Kim et al., 2023; Rumbaugh et al., 2006). However, the neuron-autonomous
100 effects of downstream ERK1/2 hyperactivation in developing cortical excitatory circuits are less
101 clear. We previously reported subtype-specific functions for ERK1/2 in the development of cortical
102 inhibitory and excitatory neurons with a series of Cre-dependent conditional mouse lines. Deletion
103 of *Mek1/2* (*Map2k1/2*) in postmitotic excitatory neurons resulted in reduced corticospinal axon
104 extension into the lumbar spinal cord followed by death of a subset of layer V CTIP2$^{+}$ neurons in
105 the neonatal motor cortex (Xing et al., 2016). In contrast, hyperactivation of ERK1/2 signaling in
106 excitatory neurons via overexpression of a Cre-dependent, phosphomimic *MEK1*$^{S217/221E}$ construct
107 did not alter CTIP2$^{+}$ density, but led to reductions in corticospinal elongation by P3 (Xing et al.,
108 2016).

109 Given the marked excitatory neuron subtype-specific outcomes associated with modifying
110 ERK1/2 activity, we sought to understand whether MEK1 hyperactivation in excitatory neurons
111 during development is sufficient to alter cortical axon outgrowth to multiple targets and ultimately
112 affect cognition. We utilized a *Nex/Neurod6:Cre* mouse to conditionally express a hyperactive
113 *MEK1*$^{S217/221E}$ construct in newborn, postmitotic cortical glutamatergic neurons, but not
114 oligodendrocytes or cortical inhibitory neurons (Goebbels et al., 2006; Krenz et al., 2008).
115 *MEK1*$^{S217/221E}$ selectively drives downstream hyperactivation of ERK1/2, independent of directly
116 manipulating parallel RTK-linked cascades. Moreover, *Nex:Cre*-directed expression minimizes
117 cellular contributions from glia and inhibitory neurons known to be modified by changes in ERK1/2
118 signaling (Angara et al., 2020; Holter et al., 2021; Kang and Lee, 2019; Knowles et al., 2023a;
119 Knowles et al., 2023b). This approach will help identify the excitatory neuron-autonomous
120 functions of selective hyperactivation of MEK-ERK1/2 signaling during long-range cortical circuit
121 formation.

122 Our results show that conditional *MEK1*$^{S217/221E}$ overexpression leads to a persistent
123 increase in phosphorylated ERK1/2 (pERK1/2) levels in axonal projections that coincides with
124 reduced motor cortex derived axon arborization in intracortical and subcortical target domains.
125 Moreover, mutant cortices exhibited reduced expression of a canonical immediate early gene,

126 Arc, and deficits in learning a single-pellet retrieval task (Guo et al., 2015; Kawai et al., 2015;
127 Peters et al., 2017; Whishaw et al., 1993). To test whether these deficits were cortical layer V-
128 autonomous, we crossed the *MEK1*$^{217/221E}$ mouse line with a *Rbp4:Cre* mouse. Viral tracing
129 analysis of contralateral corticocortical, corticostriatal, and corticospinal projections in *Rbp4:Cre*
130 *MEK1*$^{217/221E}$ mutants revealed a significant decrease in axonal innervation, but no deficit in skilled
131 motor learning. Collectively, these results indicate that excitatory neuron-specific hyperactivation
132 of MEK1 in the cortex is sufficient to disrupt the development of cortical axonal projections, the
133 expression of Arc, and select aspects of skilled motor learning.
134

135 **Materials and Methods**

136 ***Transgenic Mice***

137 All animal experiments were performed in accordance with established procedures
138 approved by the Institutional Animal Care and Use Committee of Arizona State University
139 (Protocol# 22-1924R) and NIH guidelines for the use and care of laboratory animals. Mice used
140 in this work were of a mixed genetic background, housed in standard conditions, and kept on a
141 12-hour light/dark cycle with *ad libitum* food and water. *NeuroD6/Nex-Cre (NeuroD6*$^{tm1(cre)Kan}$*)* mice
142 were kindly provided by Dr. Klaus Nave and Dr. Sandra Goebbels (MGI:2668659) (Goebbels et
143 al., 2006). *Rbp4:Cre* mice were obtained from the MMRRC (RRID:MMRRC_031125-UCD) (Gong
144 et al., 2007). *Mek1*$^{S217/221E}$ *(Tg(CAG-cat,-Map2k1*)243Rbns)* mice were provided by Dr. Maike
145 Krenz and Dr. Jeffrey Robbins (MGI:3822131) (Krenz et al., 2008). Cre-dependent *tdTomato/Ai9*
146 (B6.-Gt(ROSA)26Sor$^{tom(CAG\text{-}tdTomato)Hze}$/J) mice were ordered from Jackson Laboratories
147 (RRID:IMSR_JAX:007909) (Madisen et al., 2010). Each experiment was replicated a minimum of
148 three times from independent litters.

149 Genomic DNA was extracted from toe or tail samples and amplified with standard
150 polymerase chain reaction techniques. Primers for gene amplification are as follows 5'-3': Cre -
151 GCTAAACATGCTTCATCGTCGG and GATCTCCGGTATTGAAACTCCAGC amplify a 645 base
152 pair allele. *Mek1*$^{S217/221E}$ – GTACCAGCTCGGCGGAGACCAA and
153 TTGATCACAGCAATGCTAACTTTC amplify a 600 base pair allele. *Ai9* –
154 CTGTTCCTGTACGGCATGG and GGCATTAAAGCAGCGTATCC amplify a 196 base pair allele.

155

156 ***Tissue Preparation***

157 Transcardial perfusions were performed on mice using a 4% paraformaldehyde/PBS
158 solution and dissected brains were post-fixed overnight at 4°C. Brains were then cryopreserved
159 via serial incubations in 15% and 30% sucrose/PBS solutions prior to embedding in Tissue-Tek
160 O.C.T. (Tissue-Tek 4583) and rapid freezing. Cryostat sections were collected in cold PBS for
161 free-floating staining or mounted on Fisherbrand Superfrost Plus slides (Fisher Scientific 12-550-

162 15) and air-dried prior to staining. For vibratome sectioned material, fixed adult brains were
163 mounted in agarose and sections were collected in PBS prior to free-floating
164 immunohistochemistry.
165
166 ***Viral Injections and Image Quantification***
167 P1 pups were removed from their home cage as a group and individually cryo-
168 anesthetized on ice for 4-6 minutes. Viral injections were then performed immediately with 50nl
169 of solution using a 32-gauge beveled needle fitted to a Hamilton 5µl neuros syringe mounted on
170 a manipulator arm. After injections, pups were placed on a 37°C heated surface for recovery and
171 returned to their home cage as a group. Adeno-Associated Viral vectors containing a Cre-
172 dependent tdTomato construct under the control of a strong CAG promoter (AAV-CAG-FLEX-
173 tdTomato, UNC Viral Vector Core) were used for viral tracing experiments. For quantification of
174 virally labeled $RFP^+$ axonal arborization in the forebrain, we first manually assessed the number
175 of $RFP^+$ neurons in M1 from confocal images of at least three sections near the center of the
176 injection site. Confocal images of axonal target domains from at least three sections were
177 automatically thresholded in ImageJ using the Otsu method (Otsu, 1979). The total number of
178 $RFP^+$ pixels within the target domain was normalized to the number of labeled M1 neurons within
179 the injection site to provide a relative estimate of axonal arborization. To quantify axon elongation
180 along the spinal cord, $RFP^+$ immunolabeling in the cervical dorsal funiculus was normalized to
181 immunolabeling in hindbrain corticobulbar tract (CBT). Representative images were cropped,
182 adjusted for brightness and contrast, and inverted in Photoshop for clear visualization of axonal
183 projections.
184
185 ***Immunohistochemistry***
186 Tissue sections were rinsed with PBS/0.1% Triton X-100 (PBST) and blocked with 5%
187 normal donkey serum in PBST at room temperature for ~1 hour. Primary antibodies were diluted
188 in PBST/5%NDS and incubated overnight at 4°C with gentle agitation. Primary antibodies used

189 were: rabbit anti-MEK1 (RRID:AB776273, Abcam ab32091), rabbit anti-phospho-p44/42 MAPK
190 (ERK1/2) (Thr202/Tyr204) (RRID:AB_2315112, Cell Signaling Technologies 4370), rabbit anti-
191 ERK2 (RRID:AB_732210, Abcam ab32081), rabbit anti-ARC (RRID:AB_887694, Synaptic
192 Systems 156-003), mouse anti-β3Tubulin (TUJ1, RRID:AB_10063408, Bioloegend 801202),
193 rabbit anti-RFP (RRID:AB_2209751, Rockland 600-401-379), chicken anti-RFP
194 (RRID:AB_10704808, Rockland 600-901-379), and mouse anti-NeuN (RRID:AB_2298772,
195 Millipore Sigma MAB377). After rinsing in PBS 3X, secondary antibodies diluted in PBST/5%NDS
196 with DAPI (Sigma Aldrich 10236276001) were added and incubated overnight at 4°C with gentle
197 agitation. Secondary antibodies include Alexa Fluor 488, 546, 568, and 647 conjugated to anti-
198 rabbit IgG, anti-mouse IgG, or anti-chicken IgY (Invitrogen). Imaging was performed using a Zeiss
199 LSM 800 or Leica SP5 laser scanning confocal microscope.
200
201 ***Confocal Image Analysis and Quantification***
202 The number of pERK1/2 labeled cells in M1 layer II/III were counted from 20x confocal
203 images in at least two hemi-sections per mouse and averaged. We quantified the level of pERK1/2
204 immunolabeling in high resolution confocal images of layer V neurons collected with a 63X 1.4NA
205 objective using the same acquisition settings. Individual NeuN$^+$ pyramidal shaped somas >100
206 μm$^2$ with a clear DAPI-labeled nucleus in cortical layer V of the motor cortex were randomly
207 selected by a blinded observer. The integrated density of pERK1/2 immunolabeling in the
208 cytoplasm and nucleus was then measured. A total of 68 control and 83 mutant neurons were
209 analyzed from at least three sections per mouse, four mice per genotype, representing a total
210 sampling area >14,000 μm$^2$ per genotype.
211 To estimate the levels of pERK1/2 immunoreactivity in TUJ1$^+$ callosal axons, standard
212 confocal images of the corpus collosum were collected and analyzed. Standard confocal images
213 of at least two tissue sections of the corpus collosum per mouse were collected and automatically
214 thresholded in ImageJ in an unbiased manner using the default settings of Moments
215 Autothreshold (Tsai, 1985). Colocalized pERK1/2$^+$/TUJ1$^+$ pixels were determined using Pierre

216 Bourdoncle's Colocalization Plugin with default settings and normalized to the total number of
217 TUJ1$^{+}$ pixels. Representative images were subsequently acquired in Airyscan mode using
218 optimized settings to visualize the localization of pERK1/2 more clearly within TUJ1$^{+}$ axons.

219 To quantify CST elongation in *RBP4:Cre; Ai9*$^{+/-}$ mice, confocal images of the dorsal
220 funiculus in at least three lumbar segments per control and *MEK1*$^{S217/221E}$ expressing mice were
221 autothresholded using Moments and the relative change in the number of RFP$^{+}$ pixels was
222 determined. Representative images have been cropped and adjusted for brightness and contrast
223 in Photoshop for presentation.

224

225 ***Western Blotting***

226 Dorsal cortices were lysed in RIPA buffer (0.05M Tris-HCl, pH 7.4, 0.5M NaCl, 0.25%
227 deoxycholic acid, 1% Triton X-100, and 1 mM EDTA, Millipore) and supplemented with 0.1% SDS,
228 protease inhibitor (Sigma-Aldrich P2714), and phosphatase inhibitor cocktail II and III (Sigma-
229 Aldrich P5726) via sonication. Lysates were then cleared by centrifugation and protein
230 concentrations determined by Bradford Assay using a Peirce Protein Assay Kit (Thermo Scientific
231 23200). Equal amounts of protein were denatured in reducing sample buffer, separated by SDS-
232 PAGE gels (BioRad 456-1035 and 456-8095), and transferred to PVDF membranes (BioRad 162-
233 0177). Blots were blocked with 5% low-fat milk TBS containing 0.1% Tween-20 (TBST) for 1hr at
234 room temperature, then incubated overnight at 4°C with primary antibodies in 4% BSA in TBST.
235 Primary antibodies used were: rabbit anti-MEK1 (RRID:AB_776273, Abcam ab32091), rabbit anti-
236 phospho-p44/42 MAPK (ERK1/2) (Thr202/Tyr204) (RRID:AB_2315112, Cell Signaling
237 Technologies 4370), rabbit anti-ERK2 (RRID:AB_732210, Abcam ab32081), rabbit anti-ARC
238 (RRID:AB_887694, Synaptic Systems 156-003), rabbit anti-GAPDH (RRID:AB_561053, Cell
239 Signaling Technologies 2118), and rabbit anti-β-actin (RRID:AB_10950489, Cell Signaling
240 Technologies 8457). After washing with TBST, membranes were incubated with donkey anti-
241 rabbit HRP-conjugated secondary antibodies (Jackson Immunoresearch 711-035-152) in 5%
242 milk/TBST for 2hr at room temperature. Membranes were washed with TBST and signal was

243 detected with SuperSignal West Pico chemiluminescent (Thermo Scientific 32106) and exposed
244 to radiographic film (Thermo Scientific 34089). Quantification of Western Blots was performed
245 using a high-resolution scanned image of the exposed radiographic film in a grayscale TIFF file
246 format. Bands were selected for quantification of integrated density in ImageJ following
247 background subtraction from an unlabeled region and normalized to either the loading control or
248 non-phosphorylated target.
249

250 ***Open Field, Accelerating Rotarod, and Single-Pellet Retrieval***

251 Open field testing was performed in an open top opaque plexiglass box measuring
252 38x38x30cm. The area within the box is illuminated by a centered, overhead 40-watt spotlight.
253 Video recordings of open field behavior were scored by a blinded observer. Rotarod analysis was
254 performed on a San Diego Instruments accelerating rotarod. Animals were tested for three trials
255 per day for five consecutive days, accelerating the rotarod from 4 to 40 RPM with a 15min intertrial
256 interval. The latency to fall was measured for each of three trials during a day and averaged.

257 A single-pellet retrieval task was performed using only male mice that were acclimated to
258 sucrose pellets (TestDiet 1811555) in their home cages at least one week prior to testing. Mice
259 were habituated for 10-15min per day, for two days in the testing room and chamber, which
260 consists of a 15x10x20cm transparent acrylic box with a 5mm wide slit on the right and left side
261 of one end that opens to a 10mm high food platform. During the subsequent two training days,
262 mice were observed while single sucrose pellets were made regularly available during a 10-20min
263 session. Only mice that attempted at least 20 reaches were further analyzed. Daily testing was
264 performed for 10 min per day, for 5 days by placing a single pellet on the food platform. To
265 enhance motivation for obtaining sucrose pellets, *Nex:Cre;MEK1*$^{S217/221E}$ mice were mildly food
266 restricted by limiting free feeding to 2-6 hours daily while maintaining at least 90% of their initial
267 weight. Due to unexpected negative health effects of mild food restriction in *RBP4:Cre;*
268 *MEK1*$^{S217/221E}$ mice, these mutants and associated control mice were only restricted during a 2-4
269 hr period prior to a single 5 min session per day.

Attempts were scored as a “success” if the mouse was able to retrieve the sucrose pellet with its preferred paw and place it in its mouth. If the mouse grasped the pellet but failed to return it to its mouth, the attempt was scored as a “drop”. If the mouse clearly reached for the pellet but failed to grasp it, the attempt was categorized as a “miss”. For each mouse, the proportion of successful out of total attempts was calculated. Accelerating rotarod and single-pellet retrieval results were analyzed using a two-way repeated measures ANOVA in SPSS.

277 **Results**

278 *Hyperactivation of MEK1 increases levels of pERK1/2 in cortical excitatory neuron axons*

279 To investigate the developmental effects of excitatory neuron-autonomous hyperactive
280 MEK-ERK1/2 signaling within the cortex *in vivo*, we generated mice expressing
281 *Nex/NeuroD6:Cre*, Cre-dependent hyperactive *Mek1/Map2k1*$^{S217/221E}$, and Cre-dependent
282 tdTomato/RFP (*Ai9*$^{+/-}$) (Goebbels et al., 2006; Krenz et al., 2008; Madisen et al., 2010). As
283 expected, E14.5 *Nex:Cre; Ai9*$^{+/-}$ forebrains showed RFP expression in excitatory neurons and
284 axons in the cortical plate (CP) and intermediate zone (IZ), but not in neural stem cells in the
285 ventricular zone (VZ) (Fig. 1A-B) (Xing et al. 2016, Goebbels et al. 2006). Substantial MEK1
286 overexpression was apparent in recombined excitatory neuron somas and long-range axonal
287 projections in *Nex:Cre; MEK1*$^{S217/221E}$*; Ai9*$^{+/-}$ compared to controls (Fig. 1B-C, G-H). Western blots
288 of dorsal cortical lysates from E14.5 *Nex:Cre; MEK1*$^{S217/221E}$ embryos demonstrate a 5.29 ± 0.93
289 fold-increase in MEK1 expression relative to controls (Mean ± SEM, n=5, Student's t-test p=0.002)
290 (Fig. 1K-L).

291 *MEK1*$^{S217/221E}$ hyperphosphorylates ERK1/2 in cell free assays and in culture, but the
292 extent of downstream effects *in vivo* varies in different tissue types (Alessi et al., 1994; Bueno,
293 2000; Cowley, 1994; Klesse et al., 1999; Krenz et al., 2008; Lajiness et al., 2014; Li et al., 2012).
294 We directly measured whether excitatory neuronal *MEK1*$^{S217/221E}$ overexpression coincides with
295 increased phosphorylated ERK1/2 (pERK1/2) levels *in vivo*. E14.5 dorsal cortical lysates from
296 mutant mice exhibited a significant 1.61 ± 0.19 fold-increase in pERK1/2 levels compared to
297 controls (Mean ± SEM, n=10, Student's t-test p=0.005) (Fig. 1M-N). Immunolabeling for pERK1/2
298 in *Nex:Cre; MEK1*$^{S217/221E}$*; Ai9*$^{+/-}$ mice revealed a relative qualitative enrichment of pERK1/2 in the
299 intermediate zone and nascent RFP$^{+}$ cortical excitatory neuron axons (Fig. 1I-J, white arrows),
300 while comparable levels of pERK1/2 were observed in the unrecombined VZ of control and mutant
301 embryos.

302 We next evaluated MEK1 and pERK1/2 activation in adult brains. Adult *Nex:Cre;*
303 *MEK1*$^{S217/221E}$ cortical lysates revealed a statistically significant 1.61 ± 0.2 fold increase in MEK1

## E14.5 Cortex

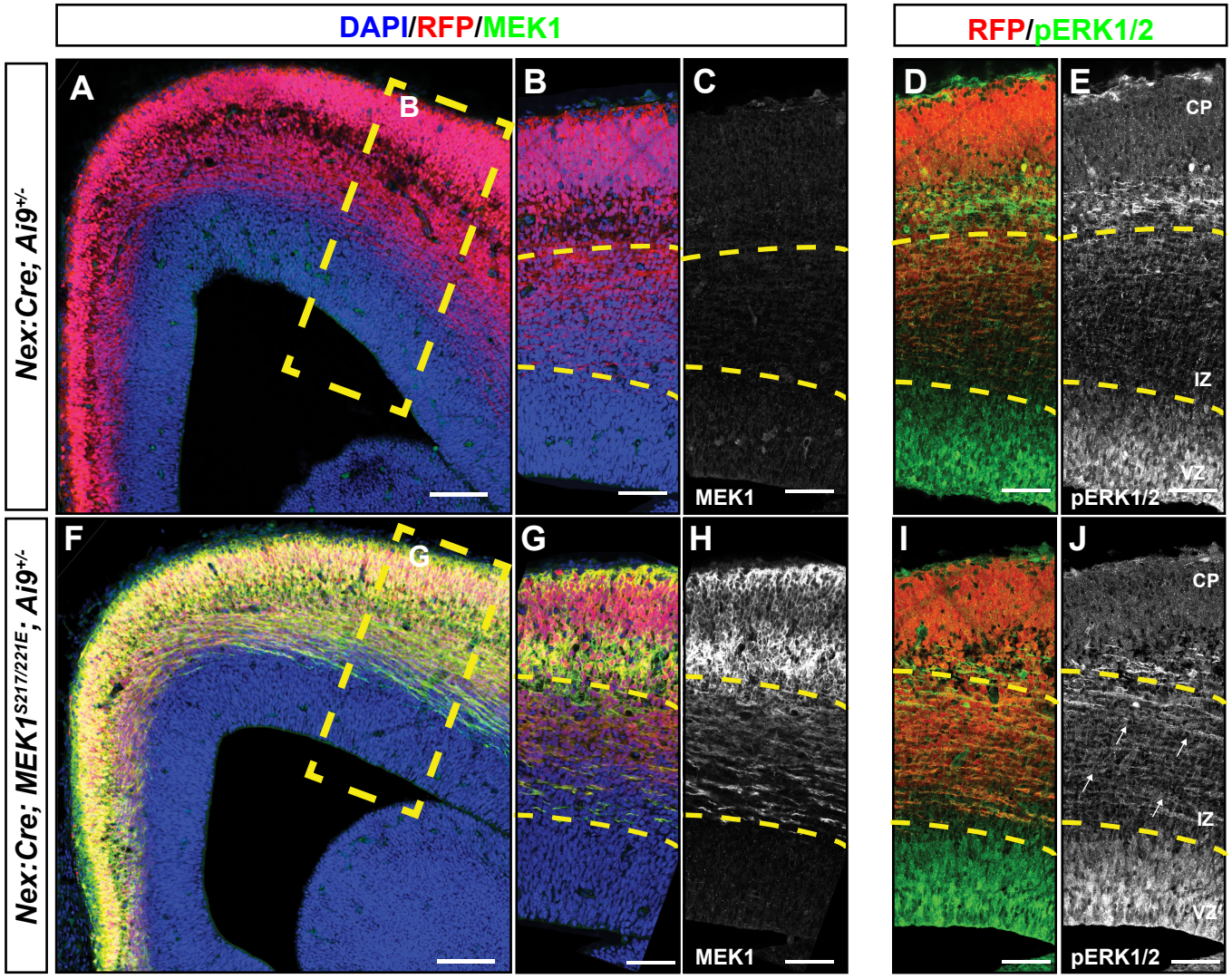
DAPI/RFP/MEK1
RFP/pERK1/2
Nex:Cre; Ai9+/-
Nex:Cre; MEK1S217/221E; Ai9+/-
A
B
C
D
E
F
G
H
I
J
MEK1
pERK1/2
CP
IZ
VZ

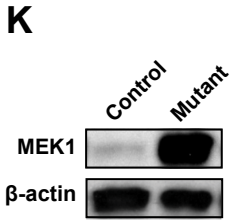
K
Control
Mutant
MEK1
β-actin

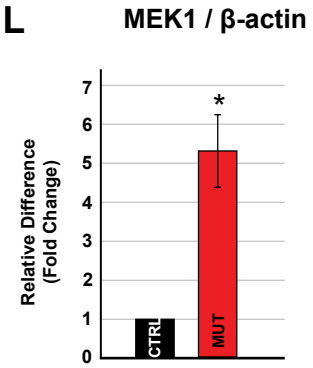
L
MEK1 / β-actin
Relative Difference (Fold Change)
0
1
2
3
4
5
6
7
*
CTRL
MUT

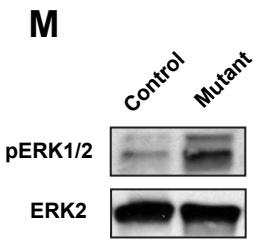
M
Control
Mutant
pERK1/2
ERK2

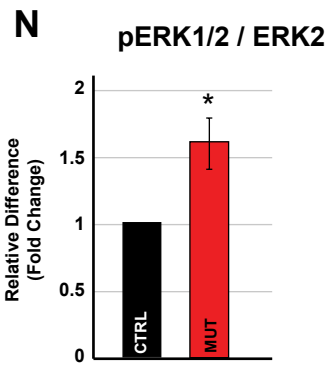
N
pERK1/2 / ERK2
Relative Difference (Fold Change)
0
0.5
1
1.5
2
*
CTRL
MUT

304 **Figure 1. MEK1 hyperactivation selectively in immature glutamatergic neurons results in**
305 **increased levels of pERK1/2 by E14.5**

306 **A-J.** Immunolabeling of E14.5 *Nex:Cre; MEK1*$^{S217/221E}$*; Ai9*$^{+/-}$ mutant cortices shows a substantial
307 increase of MEK1 expression in the intermediate zone (IZ) and cortical plate (CP) of mutants (F-
308 H) when compared to *Nex:Cre; Ai9*$^{+/-}$ controls (A-C) (n=4). RFP$^{+}$ axons within the IZ of mutants
309 (I-J, white arrow heads) exhibited a qualitative enrichment in levels of phosphorylated ERK1/2
310 relative to controls (D-E) (n=4). We did not detect a notable difference in the levels of pERK1/2 in
311 the ventricular zone (VZ), where recombination is essentially absent in these mice.

312 **K-N.** Western blots of E14.5 dorsal cortical lysates (K) reveal a 5-fold increase of MEK1 in mutants
313 compared to controls (L) (Mean ± SEM, n=5, * = Student's t-test p=0.002). We also observed a
314 significant increase in pERK1/2 levels in mutants compared to controls (M-N) (Mean ± SEM, n=10,
315 * = Student's t-test p=0.005).

316 Scale bars: A, F = 100 μm, B-E, G-J = 60μm.

317

318 expression over controls (mean ± SEM, n=3, Student's t-test p=0.041) (Fig. 2A-B). The proportion
319 of excitatory neurons in whole adult cortical lysates is relatively less than at E14.5 and may
320 contribute to the reduced fold-increase in MEK1 in adult mutants when compared to E14.5
321 mutants. We did not detect a significant difference in pERK1/2 levels between *Nex:Cre;*
322 *MEK1*$^{S217/221E}$ and control whole cortical lysates (n=3, Student's t-test p=0.832) (Fig. 2C-D). MEK1
323 immunolabeling of the cortex revealed a substantial increase in mutant excitatory neurons somas
324 and axons within the corpus callosum when compared to the controls (Fig. 2E-H).

325 Control forebrains immunolabeled for pERK1/2 showed the expected enrichment in a
326 subset of neuronal somas in layer II/III, with relative low levels in the corpus callosum (Fig. 2I-J)
327 (Hart and Balleine, 2016; Lee et al., 2021). Interestingly, in *Nex:Cre; MEK1*$^{S217/221E}$ mutant mice,
328 we observed a significant decrease in pERK1/2$^{+}$ layer II/III neurons in M1 when compared to
329 controls (n=6, Student's t test p=0.002) (Fig. 2U). Moreover, semi-quantitative high-resolution
330 analyses of pERK1/2 immunolabeling intensity in mutant layer V neurons revealed a reduction in
331 the cytoplasm and the nucleus when compared to controls (n=68 control and 83 mutant neurons
332 from four mice per genotype, Student's t-test p<0.01) (Fig. 2M-P, V). In contrast, we noted a
333 qualitative increase in pERK1/2-immunolabeling in a number of mutant forebrain white matter
334 tracts, such as the corpus callosum (Fig. 2L, yellow arrows), fimbria, and stria terminalis (Fig. S1),
335 which are enriched in axons derived from excitatory populations in the cortex, hippocampus, and
336 amygdala, respectively. High resolution analysis of pERK1/2 co-localization with TUJ1, a marker
337 of axons, in the corpus callosum, demonstrated the presence of pERK1/2 in axons and a modest
338 increase in co-localization in mutant axons compared to controls (n=4, Student's t test p = 0.054)
339 (Fig. 2Q-T, W, yellow arrows). Collectively, these data suggest glutamatergic neuron-autonomous
340 *MEK1*$^{S217/221E}$ expression results in significant hyperactivation of ERK1/2 in the axonal
341 compartment of multiple forebrain projection subtypes.

342

343 *MEK1*$^{S217/221E}$ *expression disrupts corticocortical and corticostriatal axon arborization*

344 We previously reported a reduction in corticospinal tract (CST) elongation in *Nex:Cre;*

Figure 2

## Adult Cortex

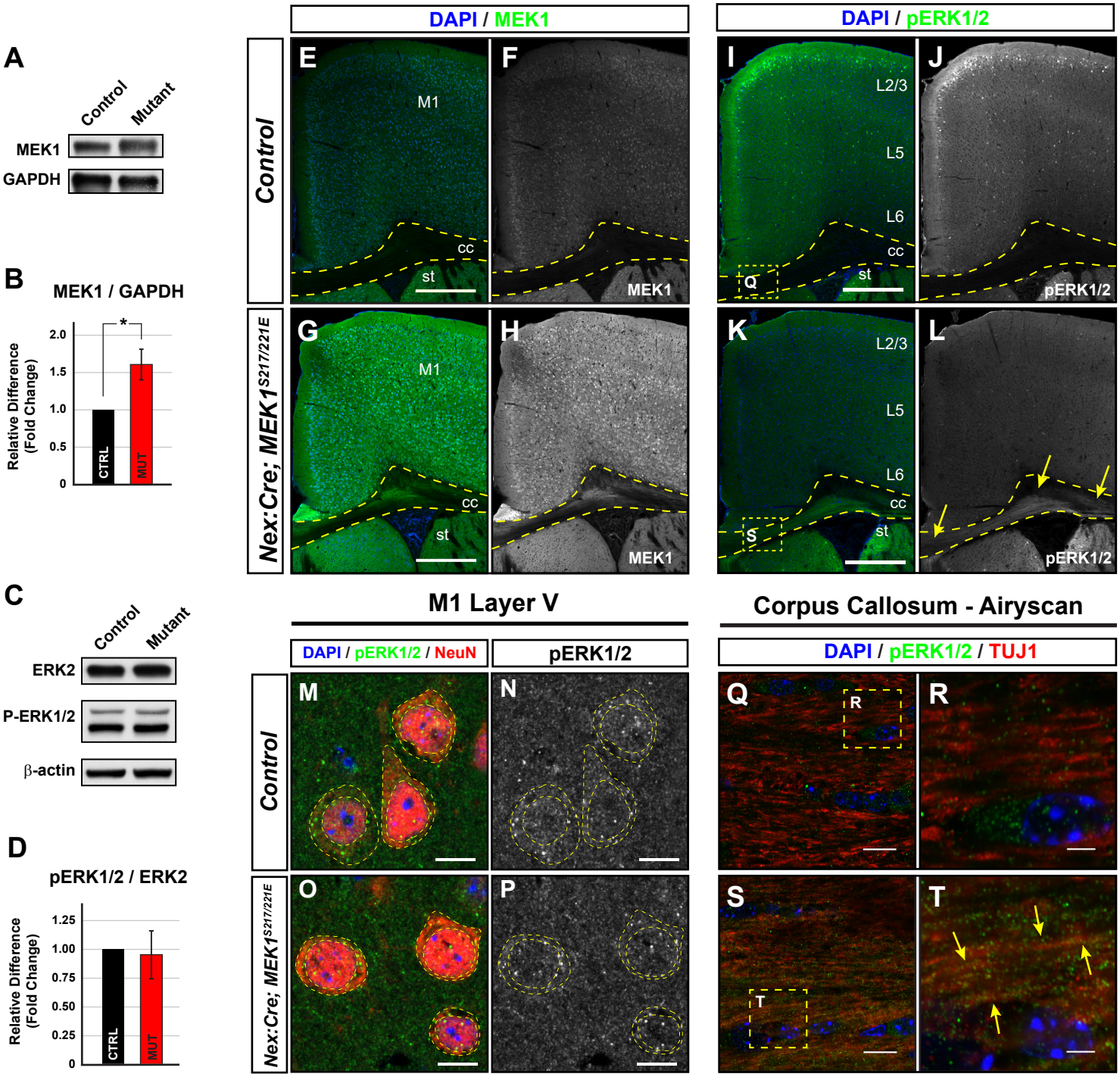

345 **Figure 2. Increased levels of pERK1/2 in cortical axons of adult Nex:Cre; MEK1$^{S217/221E}$ mice.**

346 **A-D.** Western Blots of adult cortical lysates revealed a 1.61 ± 0.20 fold increase in MEK1 in
347 *Nex:Cre; MEK1$^{S217/221E}$* mutants when compared to control mice (Mean ± SEM, n=3, Student's t-
348 test p=0.041) (A-B). No significant difference in pERK1/2 levels between mutant and control mice
349 was detected in adult cortical lysates (Mean ± SEM, n=3, Student's t-test p=0.389) (C-D).

350 **E-W.** An increase of MEK1 immunolabeling was apparent in the cortex of adult *Nex:Cre;*
351 *MEK1$^{S217/221E}$* mice (G-H) relative to controls (E-F). Phosphorylated ERK1/2 immunolabeling was
352 qualitatively increased in the corpus callosum (dotted yellow outline) in adult mutant mice (K-L,
353 yellow arrows), when compared to controls (I-J). Within the grey matter, we noted a significant
354 reduction in the number pERK1/2 labeled neurons in layer II/III of mutants (L, U) (Mean ± SEM,
355 n=6, * = Student's t test p=0.002). High resolution confocal imaging and analysis of NeuN$^{+}$
356 pyramidal neurons in M1 layer V (M-P, dotted yellow outlines) revealed a decrease in cytoplasmic
357 and nuclear levels of pERK1/2 levels (O-P, V) when compared to controls (M-N) (Mean ± SEM,
358 n=68 control and 83 mutant neurons from four mice per group, * = Student's t-test p<0.01). We
359 detected a modest increase in pERK1/2/TUJ1 co-localization in the corpus callosum of mutants
360 (S-T, yellow arrows) compared to controls (Q-R, quantified in W, Mean ± SEM, n=4, Student's t
361 test p = 0.054).

362 Scale bars E,L = 500μm, M-P = 10μm, Q-T = 2 μm (M1 = primary motor cortex, cc = corpus
363 callosum, st = striatum).

364

365 *MEK1*$^{S217/221E}$ mice by postnatal day 3 (P3) that persisted to P30 (Xing et al., 2016). Here, we
366 asked whether MEK1$^{S217/221E}$ expression is sufficient to reduce axon arborization in two other
367 target domains, the contralateral cortex and striatum. To unilaterally label developing neurons
368 and their axons, a Cre-dependent tdTomato/RFP adeno-associated viral vector (AAV-*CAG-*
369 *FLEX-tdTomato*) was injected into the primary motor cortex (M1) at P1 (Fig. 3A). There was no
370 significant difference in the density of tdTomato-labeled cells per section between *Nex:Cre;*
371 *MEK1*$^{S217/221E}$ (224.73 ± 26.73) and control (189.96 ± 14.20) motor cortices (mean ± SEM, n=5,
372 Student's t-test, p=0.284) (Fig. 3B-D). To estimate axonal arborization, tdTomato-labeled pixels
373 in contralateral M1 and striatum were quantified. There was a statistically significant reduction of
374 contralateral corticocortical arborization in *Nex:Cre; MEK1*$^{S217/221E}$ mice (631.68 ± 27.51)
375 compared to controls (791.79 ± 42.88) when normalized to number of transduced cells in M1
376 (Mean ± SEM, n=5, Student's t-test, p=0.014) (Fig. 3E, F, H, I, K). Contralateral corticostriatal
377 projections into the dorsolateral striatum were also significantly reduced in the
378 *Nex:Cre;MEK1*$^{S217/221E}$ mice (control: 255.67 ± 23.64, mutant: 155.44 ± 21.18, Mean ± SEM,
379 n=5, Student's t-test, p=0.013) (Fig. 3E, G, H, J, L). Together with our previous findings, cortical
380 glutamatergic neuron autonomous *MEK1*$^{S217/221E}$ expression appears sufficient to hyperactivate
381 ERK1/2 during axonal development and reduce arborization into multiple long-range targets.
382

383 *ARC protein levels are reduced by MEK1 hyperactivation*

384 ERK1/2 is a known regulator of glutamatergic signaling and activity dependent plasticity
385 (Bramham et al., 2010; Thomas and Huganir, 2004). Whether *MEK1*$^{S217/221E}$ expression alters
386 circuit-level cortical activity in adults is unclear. Activity-Regulated Cytoskeleton-associated gene
387 (ARC) is an immediate early gene (IEG) triggered by glutamate receptor signaling via ERK1/2
388 and other pathways (Cao et al., 2015; Chotiner et al., 2010; Correa et al., 2012; Ebert and
389 Greenberg, 2013; Pintchovski et al., 2009; Ying et al., 2002). Our data shows axonal arborization,
390 somal and nuclear levels of pERK1/2, are reduced in *Nex:Cre; MEK1*$^{S217/221E}$ mutants, suggesting

## AAV:*CAG-FLEX-tdTomato* P1 Injection: Collect P30

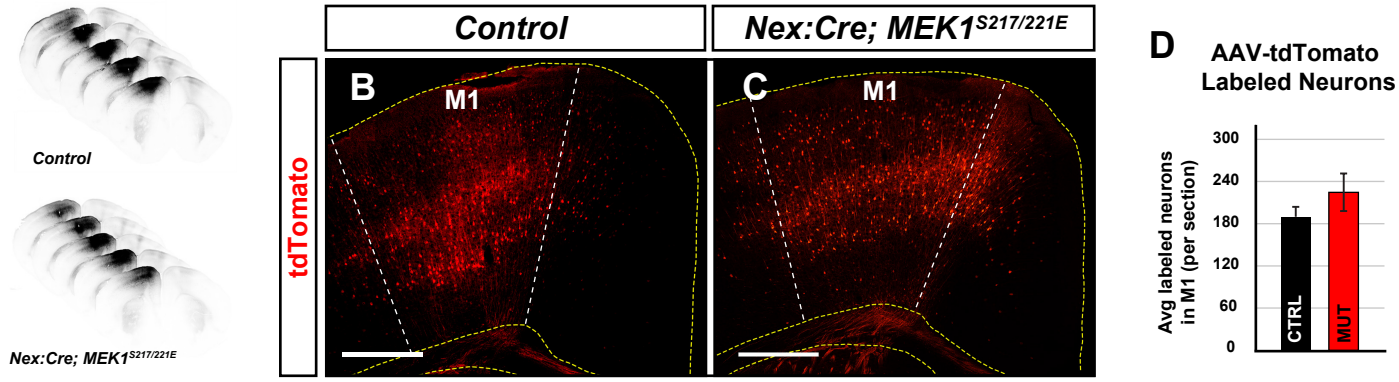


## Contralateral Corticocortical and Corticostriatal Projections

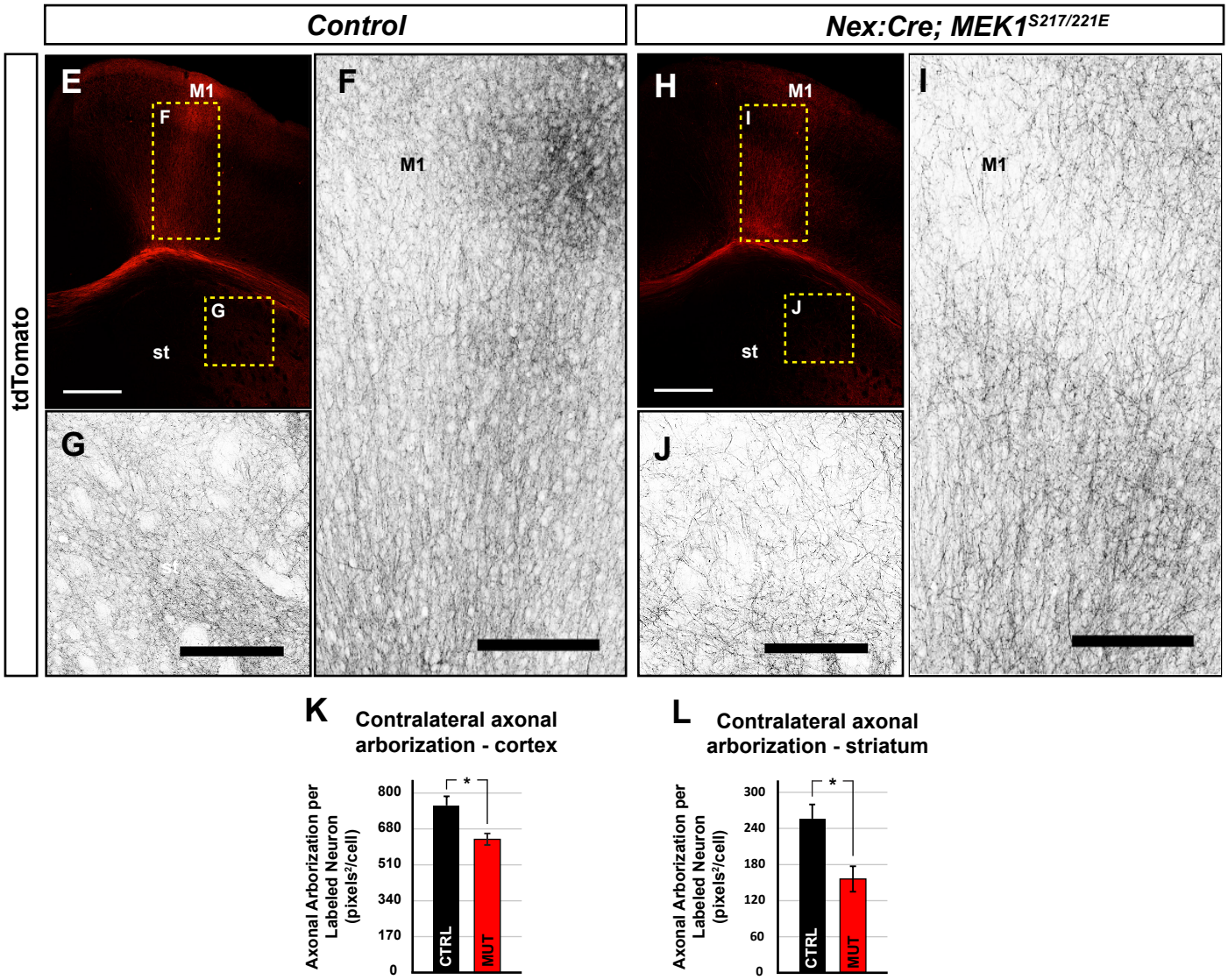

391 **Figure 3. Nex:Cre; MEK1$^{S217/221E}$ mice exhibit disrupted contralateral corticocortical and**
392 **corticostriatal arborization.**

393 **A-D.** An adeno-associated viral vector, AAV:*CAG-Flex-tdTomato* was injected into the left primary
394 motor cortex at P1 and brains were collected at P30 as shown in the rostral to caudal serial
395 sections surrounding the injection site (A) and representative images of the injected region in the
396 primary motor cortex (M1) of the *Nex:Cre; MEK1$^{S217/221E}$* (C) and control (B) forebrains. No
397 significant difference in the average density of RFP-labeled cells was detected between *Nex:Cre;*
398 *MEK1$^{S217/221E}$* and control mice (Mean ± SEM, n=5, Student's t-test p=0.2839) (D).

399 **E-L.** Representative confocal images of contralateral corticocortical and corticostriatal (st =
400 striatum) RFP-labeled axonal arborization in the *Nex:Cre; MEK1$^{S217/221E}$* (H-J) and control mice
401 (E-G). *Nex:Cre; MEK1$^{S217/221E}$* mice showed a 19.57% ± 4.30 reduction of normalized intracortical
402 axon arborization (I) compared to control mice (Mean ± SEM, n=5, Student's t-test p=0.014) (F,
403 quantified in K). Cortical axon arborization in the mutant dorsolateral striatum was reduced
404 37.50% ± 9.14 (J) compared to control mice (Mean ± SEM, n=5, Student's t-test p=0.013) (G,
405 quantified in L).

406 Scale bars: B, C, E, H = 500μm, F, G, I, J= 100μm.

407

408 that glutamatergic drive may be diminished. Indeed, western blots of adult whole cortical lysates
409 revealed a significant 37 +/- 11% decrease in ARC expression in *Nex:Cre;MEK1*$^{S217/221E}$ mice
410 compared to controls (n=11, Student's t-test p<0.005) (Fig. 4A-B). Immunolabeling further
411 indicated a widespread decrease in cortical ARC levels *in vivo* (n=4) (Fig. 4C-F). Together, these
412 findings support that developmental expression of hyperactive MEK1 in glutamatergic neurons
413 reduces cortical ARC expression *in vivo.*
414
415 *Motor skill acquisition is disrupted in Nex:Cre; MEK1*$^{S217/221E}$ *mice*
416 Common phenotypes in RASopathic individuals include hypotonia, changes in motor
417 coordination and altered motor learning (Blüthgen et al., 2017; Davis et al., 2000; Monje et al.,
418 2005). We thus asked if hyperactivation of MEK1 in *Nex:Cre* expressing cells was sufficient to
419 drive changes in adult mouse motor behavior in open field, accelerating rotarod, and single-pellet
420 retrieval assays (Crawley, 1999). Open field testing revealed no significant difference in total
421 distance traveled between *Nex:Cre; MEK1*$^{S217/221E}$ and control mice (Fig. 5A, n=12, Student's t-
422 test, p=0.075). Time spent in the center of the open field arena is a gauge of anxiety-related
423 behavior, however, we did not observe a significant difference (Fig. 5A, n=12, Student's t-test
424 p=0.21). We also did not observe a significant effect of genotype during accelerating rotarod
425 testing, which assesses motor coordination and balance (Fig. 5B, [$F_{(1, 27)}$=0.246, p=0.624], n=15
426 controls & 14 mutants). These data reveal that *Nex;Cre; MEK1*$^{S217/221E}$ mice have relatively normal
427 global voluntary locomotor behavior, motor coordination, and balance.
428 We next utilized a single-pellet retrieval task to determine if there was a deficit in fine
429 forelimb motor function and learning, which relies heavily on the motor cortex (Chen et al., 2014;
430 Kawai et al., 2015; Li and Hollis, 2021). This task assays the ability of mice to reach through a
431 narrow slot with a single forelimb to retrieve a sucrose pellet. We measured the percentage of
432 successful retrievals over the total number of reaching attempts across 5 consecutive days of
433 testing. Importantly, we found that *Nex:Cre; MEK1*$^{S217/221E}$ mutants exhibit a significant decrease

## Adult Cortex

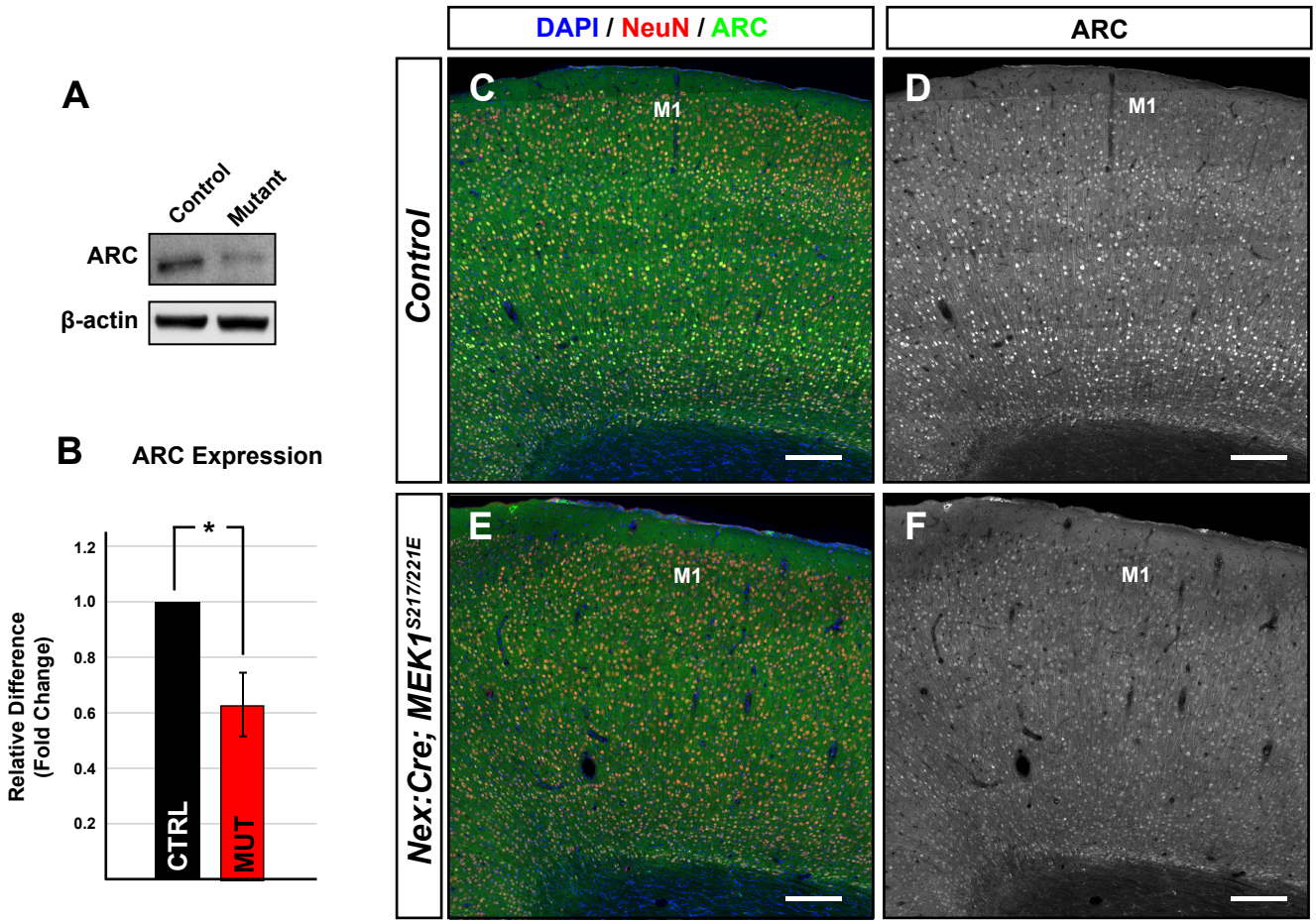

434 **Figure 4. MEK1$^{S217/221E}$ reduces cortical ARC protein expression.**

435 **A-B.** Western Blots of adult cortical lysates showed a significant reduction in ARC in *Nex:Cre;*
436 *MEK1$^{S217/221E}$* mutants when compared to control mice (Mean ± SEM, n=11, Student's t-test,
437 $p<0.005$).

438 **C-F.** Immunolabeling revealed a qualitative reduction of ARC in *Nex:Cre; MEK1$^{S217/221E}$* cortices
439 (E-F) when compared to controls (C-D, n=5).

440 Scale bars = 200um.

441

442 in success rate relative to controls (Fig. 5C, main effect of genotype [$F_{(1,16)}$=11.04, p=0.004], n=11
443 controls & 8 mutants). The success rate in mutant mice was significantly decreased relative to
444 controls during the last three days of testing ( * = LSD post-hoc p < 0.05). However, no significant
445 difference in success rate was noted on the first day of testing (LSD post-hoc p=0.59) or in the
446 number of attempts [$F_{(1,16)}$=0.06, p=0.81]. Collectively, these results indicate that the *Nex:Cre;*
447 *MEK1$^{S217/221E}$* mice do not exhibit initial, basal differences in fine forelimb motor function, but
448 display a significant impairment in learning a skilled forelimb reaching and grasping task.
449
450 *Mouse model for studying layer V autonomous effects of ERK1/2 signaling*
451 Since *Nex:Cre* recombines in all cortical layers, it is unclear whether axonal deficits are
452 due to direct layer V specific effects or changes in upstream layers in the cortical circuit. To
453 determine the layer V autonomous functions of ERK1/2 signaling, we employed a *Rbp4:Cre*
454 mouse that drives recombination primarily in cortical layer V neurons in the cortex (Gong et al.,
455 2007; Kozorovitskiy et al., 2012) and outside of the nervous system in the liver (Steinhoff et al.,
456 2021; Thompson et al., 2017). Inducible deletion of *Erk1/2* in adult mice has been shown to trigger
457 hepatocyte death and increased mortality, while ERK1/2 hyperactivation induces hepatocyte
458 proliferation and carcinoma (Cingolani et al., 2022; Huynh et al., 2003; Ito et al., 1998). Attempts
459 to generate *Rbp4:Cre; Erk1$^{-/-}$; Erk2$^{fl/fl}$* loss-of-function mice did not result in viable births (0 of 85,
460 expected 1:4 births). However, *Rbp4:Cre; MEK1$^{S217/221E}$; Ai9$^{+/-}$* mice are viable into adulthood, but
461 exhibit hepatomegaly (Fig. S2M). Nonetheless, *Rbp4:Cre; MEK1$^{S217/221E}$; Ai9$^{+/-}$* mice express RFP
462 and elevated levels of MEK1 in cortical layer V somas and axon projections and provide a model
463 for evaluating layer V-autonomous effects (Fig. S2D-F, J-L).
464
465 *Layer V directed expression of MEK1$^{S217/221E}$ reduces cortical axon arborization*
466 We did not observe a decrease in RFP$^{+}$ cortical layer V neuron density in M1 of *Rbp4:Cre;*
467 *MEK1$^{S217/221E}$; Ai9$^{+/-}$* mutants relative to controls (Control = 372 ± 9, Mutant = 477 ± 38, Mean ±

Figure 5

# Locomotor and Motor Skill Assays - *Nex:Cre; MEK1*$^{S217/221E}$

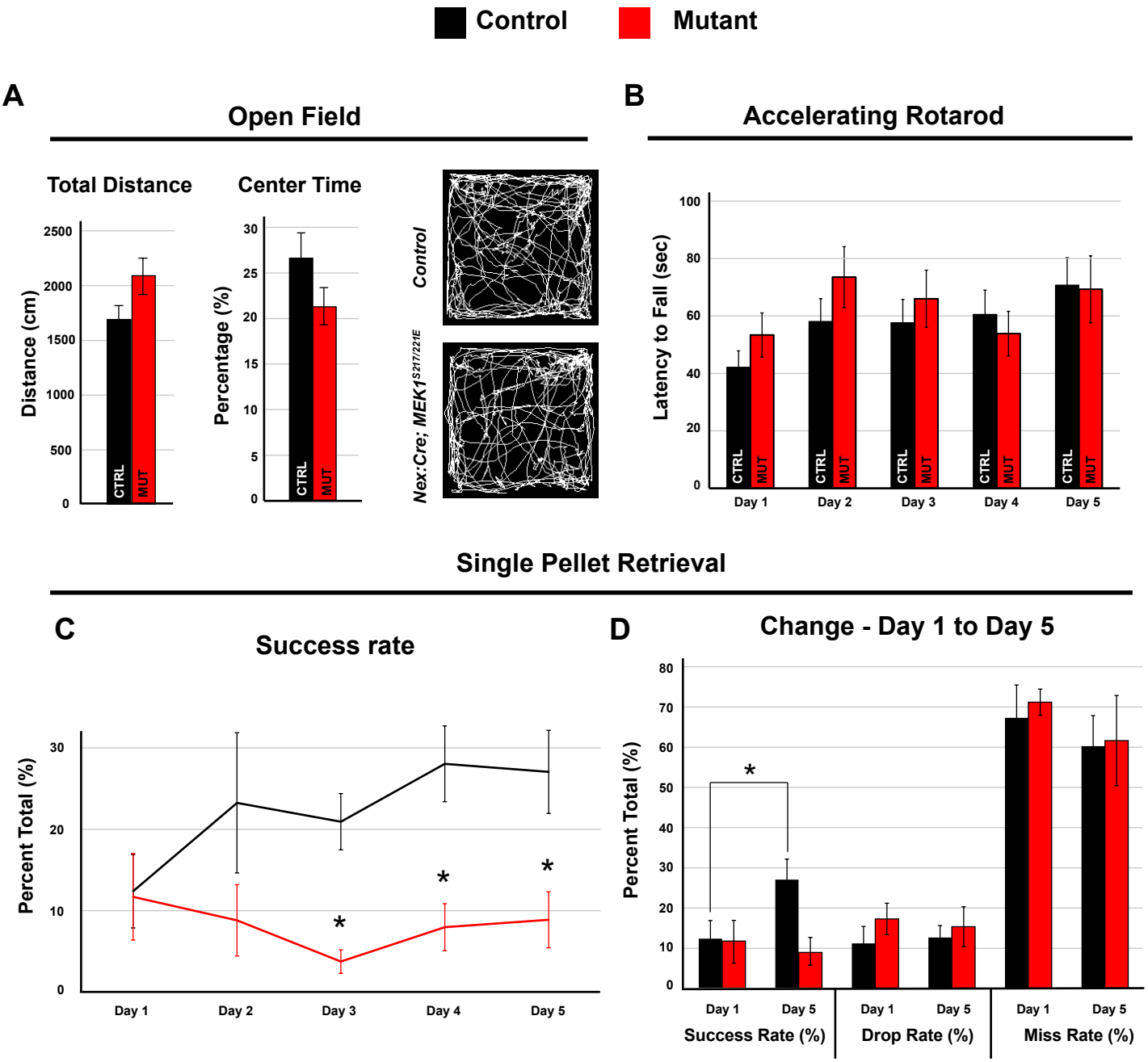

468 **Figure 5. Motor skill acquisition is disrupted by MEK1 hyperactivation in cortical**
469 **glutamatergic neurons.**

470 **A.** Open field testing of *Nex:Cre; MEK1*$^{S217/221E}$ (n=12) and control (n=12) mice revealed no
471 significant difference in distance traveled (Mean ± SEM, Student's t-test p=0.075) or time spent
472 in the center of the arena (Mean ± SEM, Student's t-test p=0.21) (A).

473 **B.** Accelerating rotarod testing revealed a significant effect of day [$F_{(4, 27)}$=6.144, p<0.001] over 5
474 days of testing, but no significant effect of genotype [$F_{(1, 27)}$=0.246, p=0.624] (Mean ± SEM, n=15
475 controls & 14 mutants) (B).

476 **C-D.** In the single-pellet retrieval task, the control success rate significantly improved over five
477 days from 12.39 ± 4.50 to 27.06 ± 5.11 percent success rate (Mean ± SEM, Students t-test D1 vs
478 D5 p=0.04, n=11) (C-D). The *Nex:Cre; MEK1*$^{S217/221E}$ mutant mice exhibited a significantly lower
479 success rate relative to controls during the final three days of testing [$F_{(1,16)}$=11.04, p=0.004] (C-
480 D, Mean ± SEM, n=11 controls & 8 mutants, * = LSD post-hoc p < 0.05).

481

482 SEM, Student's t-test p=0.054), consistent with past findings assessing the proportion of layer V
483 CTIP2$^{+}$ neurons in *Nex:Cre; MEK1$^{S217/221E}$* mice (Xing 2016) (Fig. S2B,E). We next asked if
484 hyperactive MEK1 expression in layer V is sufficient to reduce axon extension. All layer V derived
485 subcortical projections in the spinal cord dorsal funiculus were labeled by the Cre-dependent
486 tdTomato/RFP reporter, *Ai9$^{+/-}$*, in *Rbp4:Cre* mice. We observed that *Rbp4:Cre; MEK1$^{S217/221E}$;*
487 *Ai9$^{+/-}$* mice had a 28 +/- 8% reduction in RFP$^{+}$ pixel density in the lumbar dorsal funiculus
488 compared to controls (Fig. 6A-G) (Mean ± SEM, n=5, Student's t-test $p < 0.05$).

489 The widespread bilateral labeling of all cortical layer V neurons in *Rbp4:Cre; Ai9$^{+/-}$* mice
490 made it challenging to determine the anatomical source of axonal labeling. Therefore, we utilized
491 focal neonatal injection of a Cre-dependent tdTomato/RFP AAV into M1 to unilaterally label
492 neurons at birth. Comparable numbers of neurons were labeled in M1 in control and *Rbp4:Cre;*
493 *MEK1$^{S217/221E}$* mice at P30 (Mean ± SEM, n=5, Student's t-test p=0.400) (Fig. S3C). Although there
494 was no difference in RFP labeling in corticobulbar tract (CBT), mutants had reduced RFP labeling
495 in the cervical dorsal funiculus compared to controls, consistent with decreased CST elongation
496 (Fig. 7A-E, Fig. S3D-H). Intracortical arborization in contralateral M1 of *Rbp4:Cre; MEK1$^{S217/221E}$*
497 mice was also significantly reduced when compared to control mice (Mean ± SEM, n=5, Student's
498 t-test p=0.019) (Fig. 7F-G, J-K, quantification in N). Contralateral dorsolateral striatal arborization
499 was also significantly reduced in *Rbp4:Cre;MEK1$^{S217/221E}$* mice when compared to controls (Mean
500 ± SEM, n=5, Student's t-test p=0.007) (Fig. 7H-I, L-M, quantification in O). Collectively, these
501 results indicate that hyperactive ERK1/2 signaling in cortical glutamatergic layer V neurons is
502 sufficient to reduce axonal elongation of multiple projection neurons.

503

504 *Reduction in cortical wiring of layer V is expendable for skilled motor learning*

505 Since *Rbp4:Cre;MEK1$^{S217/221E}$* mice exhibit reduced axonal extension of cortical projection
506 neurons, we tested whether these mutants display deficits in motor behavior. Hepatomegaly was
507 observed in *Rbp4:Cre;MEK1$^{S217/221E}$* mice and mouse models of chronic liver disease have been
508 shown to exhibit hypolocomotion in the open-field, but little change in motor learning or anxiety-

## P60: Lumbar Spinal Cord Cre dependent tdTomato Reporter

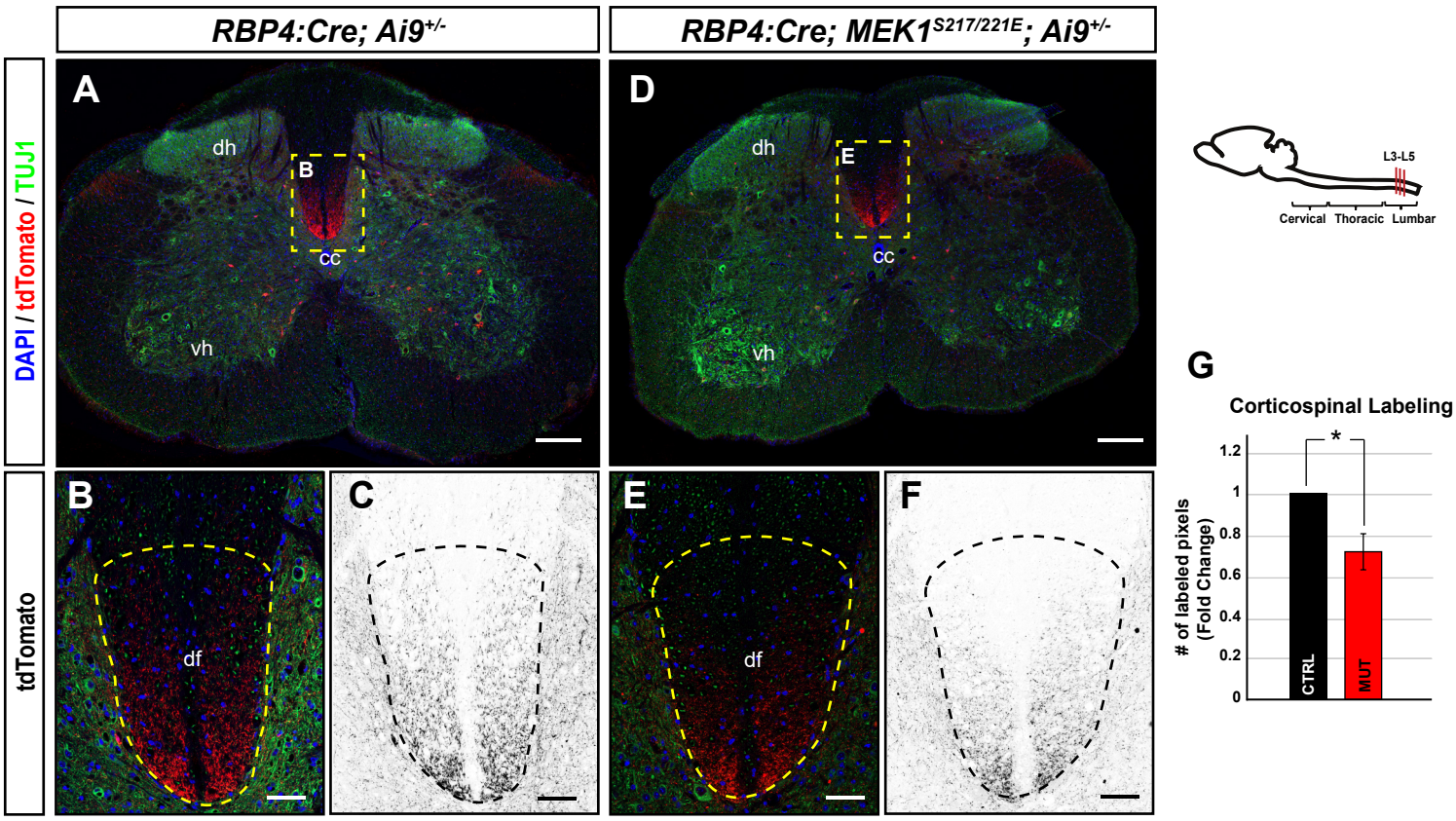

509 **Figure 6. MEK1$^{S214/221E}$ expression in cortical layer V reduces corticospinal axon elongation**
510 **in the spinal cord dorsal fasciculus.**

511 **A-G.** *RBP4:Cre; Ai9$^{+/-}$* control (A) and *RBP4:Cre; MEK1$^{S17/221E}$; Ai9$^{+/-}$* mutant (D) mice label
512 descending cortical layer V derived corticospinal axons (dotted yellow box). Cross-sectional
513 lumbar segments reveal a statistically significant 28% reduction of RFP$^{+}$ labeled pixels in the
514 dorsal funiculus of *RBP4:Cre; MEK1$^{S217/221E}$; Ai9$^{+/-}$* mice (E-F, dotted yellow outline) compared to
515 *RBP4:Cre; Ai9$^{+/-}$* controls (B-C, quantification in G, mean ± SEM, n=5, * = Student's t-test $p <$
516 0.05).

517 Scale bars A, D = 200um, B-C, E-F = 20um (dh = dorsal horn, cc = central canal, vh = ventral
518 horn, df = dorsal funiculus).

519

## AAV:*CAG-FLEX-tdTomato* P1 Injection: Collect P30

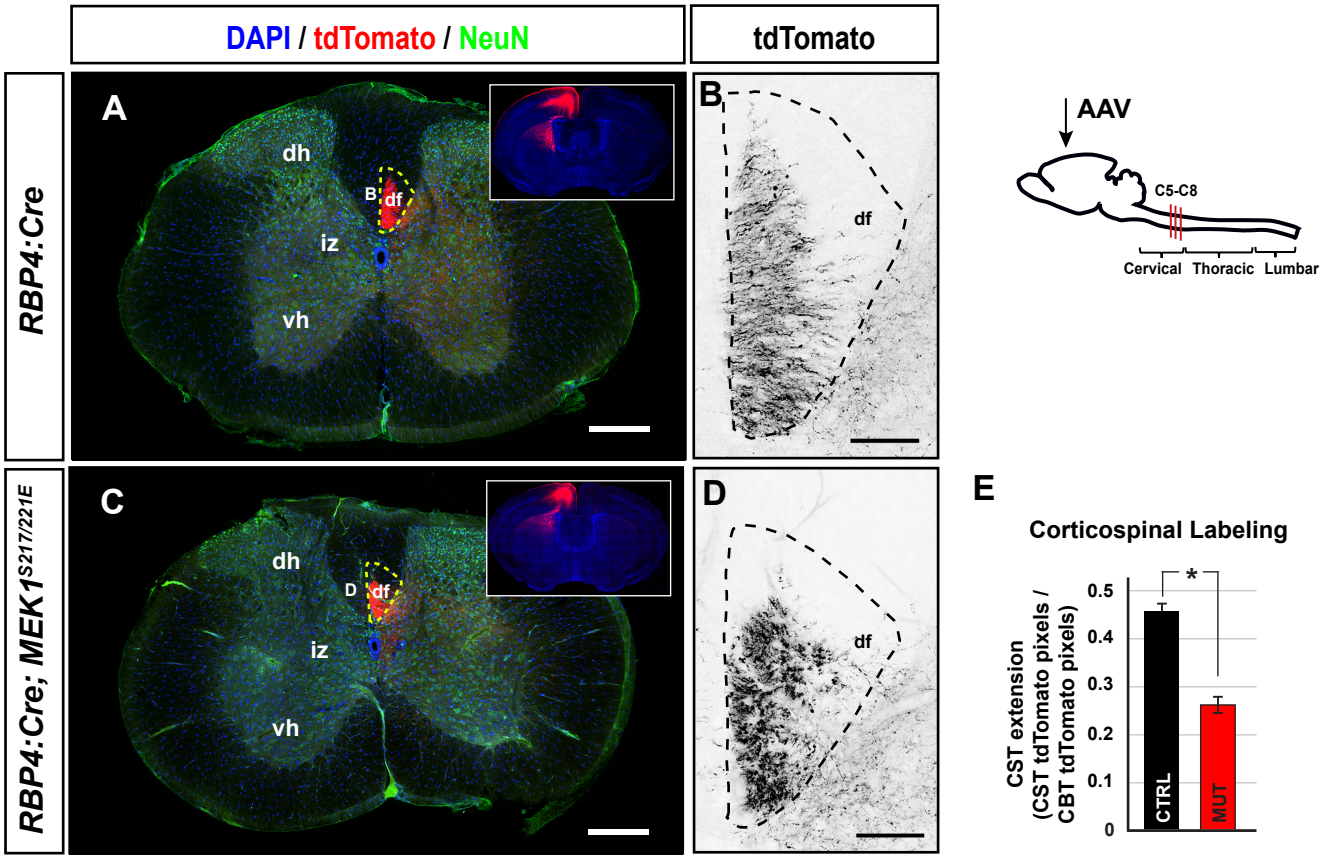


## Layer 5 Contralateral Corticocortical and Corticostriatal Projections

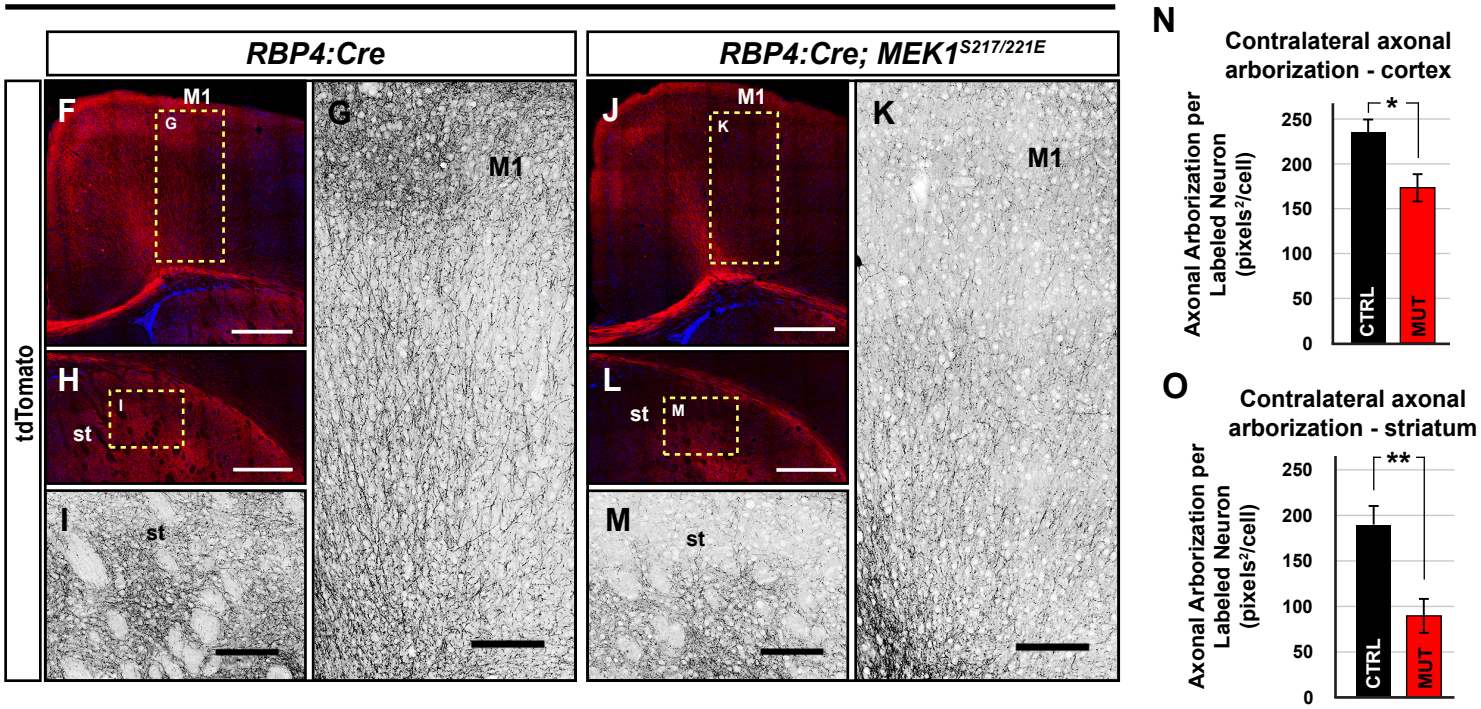

520 **Figure 7. Corticospinal, corticocortical and corticostriatal layer V projections are reduced**
521 **in *RBP4:Cre; MEK1$^{S217/221E}$* mutants.**

522 **A-E.** Unilateral AAV labeling of descending corticospinal axons derived from M1 in RBP4:Cre
523 mice. Cross sections of cervical spinal cord segments reveal a reduction of descending RFP$^{+}$
524 corticospinal axons in the dorsal funiculus of *RBP4Cre; MEK1$^{S217/221E}$* mutants (D) compared to
525 *RBP4:Cre* control mice (B) when normalized to corticobulbar tract labeling (E, Mean ± SEM, n=3,
526 Student's t-test p=0.036).

527 **F-O.** Virally-labeled *RBP4Cre; MEK1$^{S217/221E}$* axons had significantly reduced arborization in the
528 contralateral motor cortex (K) compared to *RBP4:Cre* controls (G) when normalized to the number
529 of transduced cells in M1 (quantification in N, Mean ± SEM, n=5, * = Student's t-test p=0.019).
530 Additionally, *RBP4Cre; MEK1$^{S217/221E}$* mice had significantly reduced arborization of the
531 dorsolateral striatum (M) compared to *RBP4:Cre* controls (I) (quantification in O, Mean ± SEM,
532 n=5, * Student's t-test p=0.007).

533 Scale bars: A,C, =200µm, B,D,= 20µm, F,H,J,L = 500µm, G,I,K,M = 150µm (dh = dorsal horn, df
534 = dorsal funiculus, iz = intermediate zone, vh = ventral horn, M1 = primary motor cortex, st =
535 striatum).

536

537 like phenotypes (Jover et al., 2006). When compared to control mice, *Rbp4:Cre;MEK1*$^{S217/221E}$
538 mutants showed a significant decrease in voluntary distance traveled in the open-field assay
539 (n=22 controls and 11 mutants, Student's t-test p=0.015) and a decrease in the proportion of time
540 spent in the center (Student's t-test p=0.001) (Fig. 8A). In contrast, no significant effect of
541 genotype was detected on the accelerating rotarod task ([$F_{(1,36)}$=0.007, p=0.933], n=26 controls &
542 12 mutants) (Fig. 8B).

543 In the single-pellet retrieval task, we found that mild food restriction in *Rbp4:Cre;*
544 *MEK1*$^{S217/221E}$ mice resulted in health issues of unknown origin and spontaneous lethality. Thus,
545 we substantially reduced the period of food restriction relative to our *Nex:Cre* experiments and
546 only analyzed reaching and grasping behaviors during the first five minutes of each trial when
547 mice were highly motivated. In stark contrast to *Nex:Cre; MEK1*$^{S217/221E}$ mutants, we found no
548 significant effect of genotype on the success rate between control and *Rbp4:Cre;MEK1*$^{S217/221E}$
549 mice (Fig. 8C-D, ([$F_{(1,24)}$=0.03, p=0.88], n=14 controls & 12 mutants). Taken together, these
550 results indicate that layer V specific hyperactivation of MEK1 in glutamatergic neurons is
551 insufficient to disrupt motor skilled learning.
552

Figure 8

# Locomotor and Motor Skill Assays - *RBP4:Cre; MEK1*$^{S217/221E}$

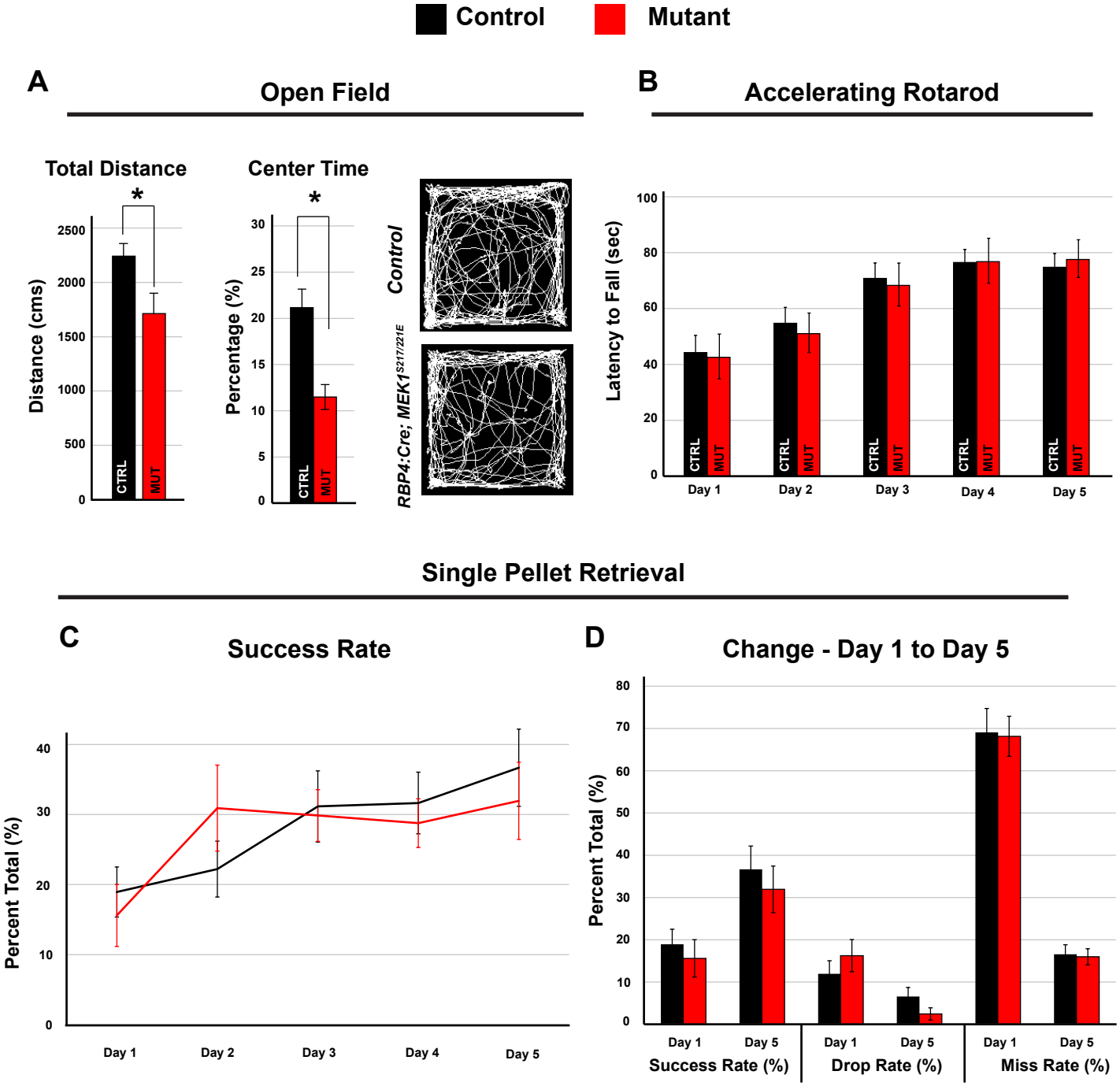

553 **Figure 8. MEK1$^{S217/221E}$ in cortical layer V glutamatergic neurons does not disrupt motor**
554 **learning.**

555 **A.** Open field testing of RBP4*:Cre; MEK1$^{S217/221E}$* and control mice revealed that mutants exhibit
556 a significant reduction in total distance traveled (Mean ± SEM, n= 22 controls & 11 mutants,
557 Student's t-test p=0.01) and time spent in center of box (Mean ± SEM, n= 22 controls & 11
558 mutants, Student's t-test p=0.001).

559 **B.** Accelerating rotarod testing revealed no significant effect of genotype over 5 days of testing
560 control and mutant mice ([$F_{(1,36)}$=0.007, p=0.933] (Mean ± SEM , n=26 controls & 12 mutants).

561 **C-D.** In the single-pellet retrieval task, there was no significant effect of genotype on daily success
562 rate [$F_{(1,24)}$=0.03, p=0.88] (C, Mean ± SEM, n=14 controls & 12 mutants). Both mutants and
563 controls improved their success rate over five days [$F_{(4,24)}$=5.81, p<0.01] (D, Mean ± SEM, n = 14
564 controls & 12 mutants).

565

566 **Discussion**

567 Resolving the cell-specific effects of pathological ERK1/2 activity may help inform the
568 rational design of therapeutic approaches for multiple neurodevelopmental conditions. Here, we
569 tested whether cortical excitatory neuron-directed expression of hyperactive MEK1$^{S217/221E}$ during
570 early development modulates long-range axon outgrowth from sensorimotor cortices, expression
571 of ARC, and motor-related behaviors. MEK1 hyperactivation selectively mimics a core
572 downstream feature of multiple RASopathies without direct modulation of multiple RTK-linked
573 signaling cascades associated with upstream mutations. We generated mice expressing Cre-
574 dependent MEK1$^{S217/221E}$ and *Nex:Cre* to target cortical excitatory neurons, but not cortical
575 GABAergic neurons or glia. Axonal levels of pERK1/2 are persistently increased in these mutants.
576 Importantly, ERK1/2 hyperactivation coincides with reductions in corticocortical, corticostriatal,
577 and corticospinal axon projections arising from motor cortices. We also observe lower expression
578 of the activity-dependent gene, Arc, within the mature cortex of mutant mice. While many basic
579 motor behaviors remain intact, skilled motor learning in a reaching task is inhibited in these
580 mutants. Lastly, we demonstrate that a layer V-specific MEK1$^{S217/221E}$ mutant mouse recapitulates
581 axonal outgrowth deficits, but motor learning is not altered. Overall, our data show that layer V
582 autonomous expression of MEK1$^{S217/221E}$ disrupts the development of long-range cortical axon
583 projections, while MEK1 hyperactivation in developing *Nex:Cre*-expressing neurons appears
584 necessary for diminished skilled motor learning (Fig. S4).

585

586 **Compartment-specific ERK1/2 activation in *MEK1$^{S217/221E}$*-expressing neurons**

587 *In vitro* studies have been vital for quantitative studies of kinase signaling and
588 pharmacological inhibitors, but the precise effect of RASopathy mutations on pERK1/2 levels and
589 distribution are more challenging to measure *in vivo*. We generated mutants with increased
590 hyperactive MEK1 levels in developing excitatory neurons and observed increased levels of
591 pERK1/2 in axonal, but not somal and nuclear compartments. Recent studies have shown that
592 callosal layer II/III projections have enriched ERK2/MAPK1 protein within axonal growth cones

593 (Engmann et al., 2022; Poulopoulos et al., 2019; Shigeoka et al., 2016). It will be important to
594 explore whether enrichment of ERK1/2 pathway components within the axon renders this
595 compartment relatively vulnerable to RASopathic mutations. High resolution measurement of
596 RASopathic kinase activation in distinct subcellular domains *in vivo* may further illuminate core
597 pathological mechanisms.

598 Paradoxically, the somal and nuclear levels of pERK1/2 were reduced in adult mutant
599 excitatory neurons. A similar phenomenon has been observed in Drosophila MEK1 mutants,
600 possibly due to early changes in the expression of morphogens during development (Goyal et al.,
601 2017). The compensatory mechanisms that appear to override the biochemical hyperactivity of
602 the MEK1$^{S217/221E}$ mutant in neuronal soma and nuclei may involve ERK1/2-directed
603 phosphatases enriched within somal compartments or developmental changes in upstream
604 ERK1/2 activators (Caunt et al., 2008; Jeffrey et al., 2007; Li et al., 2007; Lim et al., 2015; Parmar
605 et al., 2015; Poulopoulos et al., 2019). Nevertheless, pharmacological inhibitors of the ERK1/2
606 signaling cascade are actively being explored for clinical use in RASopathies (Guilding et al.,
607 2007; Hatzivassiliou et al., 2010; Morris et al., 2013; Nakamura et al., 2009; Zamorano et al.,
608 2018). For example, MEK1/2 inhibitors during postnatal stages reverses cardiac deficits and
609 tumorigenesis in RASopathy models and patients with Noonan Syndrome (Andelfinger et al.,
610 2019; Hilal et al., 2023; Wu et al., 2011). However, if developmental compensatory mechanisms
611 lead to paradoxically reduced levels of pERK1/2 in select neuronal compartments, it is unclear
612 whether pharmacological inhibition would be beneficial. Additional quantitative analyses of
613 compartment-specific changes in pERK1/2 levels in RASopathy models may help inform the use
614 of systemic pharmacological inhibitors.

615

616 **MEK-ERK1/2 hyperactivity reduces cortical long-range axon arborization**

617 MRI-based studies of individuals with NF1 and Noonan Syndrome have discovered
618 abnormalities in both functional and structural connectivity (Fattah et al., 2021; Filippi et al., 2013;
619 Rai et al., 2023). While oligodendrocyte mediated changes in the myelination of axons are likely

620 involved, the neuron-autonomous contributions to aberrant connectivity are less understood. We
621 show that neuron-specific MEK1$^{S217/221E}$ expressing mice did not exhibit significant loss of cortical
622 layer V neurons, but layer V-autonomous hyperactivation of ERK1/2 reduces the arborization of
623 corticocortical, corticostriatal, and corticospinal axons. *In vitro* studies have demonstrated ERK1/2
624 is necessary for aspects of trophic factor-induced axon outgrowth (Markus et al., 2002; Ozdinler
625 and Macklis, 2006), axon guidance (Bagnard et al., 2004; Forcet et al., 2002; Yun et al., 2005),
626 cytoskeletal organization (Atwal et al., 2003; Goold and Gordon-Weeks, 2005; Ray and Sturgill,
627 1987) and local protein translation in growth cones (Campbell and Holt, 2003). Whether
628 hyperactive ERK1/2 activity disrupts these molecular processes or modulates other intracellular
629 events associated with axon outgrowth *in vivo* is unclear. Axonal outgrowth in humans occurs
630 during gestational stages, which makes therapeutic intervention more difficult. RASopathies are
631 often diagnosed within the first years of life (Zenker et al., 2022). Therefore, it may be beneficial
632 to study postnatal stages of axonal refinement and pruning in RASopathies, which may be more
633 accessible to current treatment strategies.

634 Animal models of upstream RASopathic mutations in NF1, Ptpn11, and Ras have
635 observed changes in multiple RTK-linked downstream intracellular cascades, including PI3K/Akt,
636 JAK/STAT, PKC, mTOR and ERK1/2, and inhibitors of multiple cascades are capable of reversing
637 certain cellular deficits (Anastasaki and Gutmann, 2014; Brown et al., 2012; Langdon et al., 2012;
638 López-Juárez et al., 2017; Titus et al., 2017). Our work now shows that downstream MEK-ERK1/2
639 hyperactivity is sufficient to reduce long range axon arborization *in vivo*. Understanding whether
640 upstream mutations also drive neuron-autonomous deficits in long-range excitatory neuron
641 axonal outgrowth and may help inform the design of personalized, mutation-specific approaches
642 to RASopathy therapeutics.

643

644 **Nex:Cre; MEK1$^{S217/221E}$ mice exhibit decreased Arc and deficits in skilled motor learning**

645 Activity-regulated cytoskeletal gene *Arc* is an immediate early gene that rapidly responds
646 to neuronal activity and regulates synaptic plasticity (Steward and Worley, 2001; Steward et al.,

647 1998). *Arc* has been shown to be dysregulated in Fragile X and Angelman Syndrome (Greer et
648 al., 2010; Zalfa et al., 2003), however, whether RASopathic individuals exhibit aberrant *Arc*
649 expression is not clear. Several reports show that glutamate and BDNF drive Arc transcription
650 and translation via ERK1/2 (Chotiner et al., 2010; Correa et al., 2012; Nikolaienko et al., 2017;
651 Pintchovski et al., 2009; Rao et al., 2006; Ying et al., 2002). Notably, our results indicate that
652 MEK1 hyperactivation during early neuronal development unpredictably resulted in reduced
653 phosphorylated ERK1/2 levels in the soma and nucleus of adult neurons. It is perhaps not
654 surprising that ARC protein is also decreased in adult mutant cortices, in agreement with our
655 past report showing P21 *Nex:Cre; MEK1*$^{S217/221E}$ mice have reduced levels of *Arc* mRNA (Xing
656 et al., 2016). Hippocampal excitatory neurons in a developing forebrain-directed RASopathy
657 mutant, *Emx1:Cre Ptpn11*$^{D61Y}$, exhibit analogous reductions in depolarization-induced pERK1/2
658 and BDNF promoter activity (Altmüller et al., 2017). We propose the reduced levels of pERK1/2-
659 ARC in cortical neuron soma and nuclei may be due to decreases in the development of cortical
660 glutamatergic synapses or excitatory activity as a consequence of diminished long-range axon
661 outgrowth.

662 In line with the reduced expression of *Arc*, our data show that *MEK1*$^{S217/221E}$ expression in
663 *Nex:Cre* mice is sufficient to disrupt skilled motor learning. *Nex/Neurod6* predominantly drives
664 Cre expression in immature cortical excitatory neurons, however, we cannot exclude that other
665 *Nex/Neurod6* expressing neuronal populations could contribute to this behavioral phenotype
666 (Goebbels et al., 2006). Nonetheless, restricting MEK1$^{S217/221E}$ to layer V with *Rbp4:Cre* does not
667 result in decreased skilled motor learning even though we observed a decrease in layer V neuron
668 axon outgrowth. Motor learning is known to involve a complex, distributed set of neuronal
669 populations that are not targeted in *Rbp4:Cre* mice. For example, the activity of layer II/III neurons
670 in the motor cortex are recruited in a skilled reaching task and contain a sparse population of
671 pyramidal neurons with some of the highest levels of pERK1/2 in the normal adult mouse cortex
672 (Levy et al., 2020). We found a reduction in the number of layer II/III neurons with high levels of
673 pERK1/2 in the motor cortex of *Nex:Cre; MEK1*$^{S217/221E}$ mice. Additional research is needed to

explore the normal functions of these high pERK1/2-expressing layer II/III neurons in cortical processes and whether they are particularly vulnerable to RASopathic signaling.

***Funding***

This work was supported by the National Institutes of Health [K99/R00 NS076661 and R01 NS097537 to JMN].

***Acknowledgments***

We wish to thank Noah Fry, Becca Reinking-Herd, and Sarah Bjorklund, for their technical assistance.

***References***


Alessi, D. R., Saito, Y., Campbell, D. G., Cohen, P., Sithanandam, G., Rapp, U., Ashworth, A., Marshall, C. J. and Cowley, S. (1994). Identification of the sites in MAP kinase kinase-1 phosphorylated by p74raf-1. *The EMBO Journal* 13, 1610–1619.

Altmüller, F., Pothula, S., Annamneedi, A., Nakhaei-Rad, S., Montenegro-Venegas, C., Pina-Fernández, E., Marini, C., Santos, M., Schanze, D., Montag, D., et al. (2017). Aberrant neuronal activity-induced signaling and gene expression in a mouse model of RASopathy. *PLoS Genet* 13, e1006684.

Anastasaki, C. and Gutmann, D. H. (2014). Neuronal NF1/RAS regulation of cyclic AMP requires atypical PKC activation. *Human Molecular Genetics* 23, 6712–6721.

Andelfinger, G., Marquis, C., Raboisson, M.-J., Théoret, Y., Waldmüller, S., Wiegand, G., Gelb, B. D., Zenker, M., Delrue, M.-A. and Hofbeck, M. (2019). Hypertrophic Cardiomyopathy in Noonan Syndrome Treated by MEK-Inhibition. *J Am Coll Cardiol* 73, 2237–2239.

Angara, K., Pai, E. L.-L., Bilinovich, S. M., Stafford, A. M., Nguyen, J. T., Li, K. X., Paul, A., Rubenstein, J. L. and Vogt, D. (2020). *Nf1* deletion results in depletion of the *Lhx6* transcription factor and a specific loss of parvalbumin $^{+}$ cortical interneurons. *Proc. Natl. Acad. Sci. U.S.A.* 117, 6189–6195.

Atkins, C. M., Yon, M., Groome, N. P. and Sweatt, J. D. (2001). Regulation of Myelin Basic Protein Phosphorylation by Mitogen-Activated Protein Kinase During Increased Action Potential Firing in the Hippocampus. *Journal of Neurochemistry* 73, 1090–1097.

Atwal, J. K., Singh, K. K., Tessier-Lavigne, M., Miller, F. D. and Kaplan, D. R. (2003). Semaphorin 3F Antagonizes Neurotrophin-Induced Phosphatidylinositol 3-Kinase and Mitogen-Activated Protein Kinase Kinase Signaling: A Mechanism for Growth Cone Collapse. *The Journal of Neuroscience* 23, 7602–7609.

Aydin, S., Kurtcan, S., Alkan, A., Guler, S., Filiz, M., Yilmaz, T. F., Sahin, T. U. and Aralasmak, A. (2016). Relationship between the corpus callosum and neurocognitive disabilities in children with NF-1: diffusion tensor imaging features. *Clinical Imaging* 40, 1092–1095.

Bagnard, D., Sainturet, N., Meyronet, D., Perraut, M., Miehe, M., Roussel, G., Aunis, D., Belin, M. F. and Thomasset, N. (2004). Differential MAP kinases activation during semaphorin3A-induced repulsion or apoptosis of neural progenitor cells. *Mol Cell Neurosci* 25, 722–731.

Bernardino, I., Dionísio, A. and Castelo-Branco, M. (2022). Cortical inhibition in neurofibromatosis type 1 is modulated by lovastatin, as demonstrated by a randomized, triple-blind, placebo-controlled clinical trial. *Sci Rep* 12, 13814.

Blüthgen, N., van Bentum, M., Merz, B., Kuhl, D. and Hermey, G. (2017). Profiling the MAPK/ERK dependent and independent activity regulated transcriptional programs in the murine hippocampus in vivo. *Sci Rep* 7, 45101.

Bramham, C. R., Alme, M. N., Bittins, M., Kuipers, S. D., Nair, R. R., Pai, B., Panja, D., Schubert, M., Soule, J., Tiron, A., et al. (2010). The Arc of synaptic memory. *Exp Brain Res* 200, 125–140.

Brown, J. A., Diggs-Andrews, K. A., Gianino, S. M. and Gutmann, D. H. (2012). Neurofibromatosis-1 heterozygosity impairs CNS neuronal morphology in a cAMP/PKA/ROCK-dependent manner. *Molecular and Cellular Neuroscience* 49, 13–22.

Bueno, O. F. (2000). The MEK1-ERK1/2 signaling pathway promotes compensated cardiac hypertrophy in transgenic mice. *The EMBO Journal* 19, 6341–6350.

Campbell, D. S. and Holt, C. E. (2003). Apoptotic Pathway and MAPKs Differentially Regulate Chemotropic Responses of Retinal Growth Cones. *Neuron* 37, 939–952.

Cao, V. Y., Ye, Y., Mastwal, S., Ren, M., Coon, M., Liu, Q., Costa, R. M. and Wang, K. H. (2015). Motor Learning Consolidates Arc-Expressing Neuronal Ensembles in Secondary Motor Cortex. *Neuron* 86, 1385–1392.

Castellano, E. and Downward, J. (2011). RAS Interaction with PI3K: More Than Just Another Effector Pathway. *Genes Cancer* 2, 261–274.

Caunt, C. J., Armstrong, S. P., Rivers, C. A., Norman, M. R. and McArdle, C. A. (2008). Spatiotemporal Regulation of ERK2 by Dual Specificity Phosphatases. *Journal of Biological Chemistry* 283, 26612–26623.

Chang, Y. S., Owen, J. P., Pojman, N. J., Thieu, T., Bukshpun, P., Wakahiro, M. L. J., Marco, E. J., Berman, J. I., Spiro, J. E., Chung, W. K., et al. (2016). Reciprocal white matter alterations due to 16p11.2 chromosomal deletions versus duplications: White Matter Microstructure in 16p11.2 CNVs. *Hum. Brain Mapp.* 37, 2833–2848.

Chen, C.-C., Gilmore, A. and Zuo, Y. (2014). Study Motor Skill Learning by Single-pellet Reaching Tasks in Mice. *JoVE* 51238.

Chotiner, J. K., Nielson, J., Farris, S., Lewandowski, G., Huang, F., Banos, K., de Leon, R. and Steward, O. (2010). Assessment of the role of MAP kinase in mediating activity-dependent transcriptional activation of the immediate early gene *Arc/Arg3.1* in the dentate gyrus in vivo. *Learn. Mem.* 17, 117–129.

Chung, W. K., Roberts, T. P., Sherr, E. H., Snyder, L. G. and Spiro, J. E. (2021). 16p11.2 deletion syndrome. *Current Opinion in Genetics & Development* 68, 49–56.

Cingolani, F., Liu, Y., Shen, Y., Wen, J., Farris, A. B. and Czaja, M. J. (2022). Redundant Functions of ERK1 and ERK2 Maintain Mouse Liver Homeostasis Through Down-Regulation of Bile Acid Synthesis. *Hepatology Communications* 6, 980–994.

Clement, J. P., Aceti, M., Creson, T. K., Ozkan, E. D., Shi, Y., Reish, N. J., Almonte, A. G., Miller, B. H., Wiltgen, B. J., Miller, C. A., et al. (2012). Pathogenic SYNGAP1 mutations impair cognitive development by disrupting maturation of dendritic spine synapses. *Cell* 151, 709–723.

Correa, S. A. L., Hunter, C. J., Palygin, O., Wauters, S. C., Martin, K. J., McKenzie, C., McKelvey, K., Morris, R. G. M., Pankratov, Y., Arthur, J. S. C., et al. (2012). MSK1 Regulates Homeostatic and Experience-Dependent Synaptic Plasticity. *Journal of Neuroscience* 32, 13039–13051.

Cowley, S. (1994). Activation of MAP kinase kinase is necessary and sufficient for PC12 differentiation and for transformation of NIH 3T3 cells. *Cell* 77, 841–852.

Crawley, J. N. (1999). Behavioral phenotyping of transgenic and knockout mice: experimental design and evaluation of general health, sensory functions, motor abilities, and specific behavioral tests1Published on the World Wide Web on 2 December 1998.1. *Brain Research* 835, 18–26.

Cui, Y., Costa, R. M., Murphy, G. G., Elgersma, Y., Zhu, Y., Gutmann, D. H., Parada, L. F., Mody, I. and Silva, A. J. (2008). Neurofibromin regulation of ERK signaling modulates GABA release and learning. *Cell* 135, 549–560.

Davis, S., Vanhoutte, P., Pages, C., Caboche, J. and Laroche, S. (2000). The MAPK/ERK cascade targets both Elk-1 and cAMP response element-binding protein to control long-term potentiation-dependent gene expression in the dentate gyrus in vivo. *The Journal of neuroscience : the official journal of the Society for Neuroscience* 20, 4563–4572.

Doherty, A. C., Huddleston, D. A., Horn, P. S., Ratner, N., Simpson, B. N., Schorry, E. K., Aschbacher-Smith, L., Prada, C. E. and Gilbert, D. L. (2023). Motor Function and Physiology in Youth With Neurofibromatosis Type 1. *Pediatr Neurol* 143, 34–43.

Ebert, D. H. and Greenberg, M. E. (2013). Activity-dependent neuronal signalling and autism spectrum disorder. *Nature* 493, 327–337.

Engmann, A. K., Hatch, J. J., Nanda, P., Veeraraghavan, P., Ozkan, A., Poulopoulos, A., Murphy, A. J. and Macklis, J. D. (2022). Neuronal subtype-specific growth cone and soma purification from mammalian CNS via fractionation and fluorescent sorting for subcellular analyses and spatial mapping of local transcriptomes and proteomes. *Nat Protoc* 17, 222–251.

Fattah, M., Raman, M. M., Reiss, A. L. and Green, T. (2021). PTPN11 Mutations in the Ras-MAPK Signaling Pathway Affect Human White Matter Microstructure. *Cerebral Cortex* 31, 1489–1499.

Filippi, C. G., Watts, R., Duy, L. A. N. and Cauley, K. A. (2013). Diffusion-Tensor Imaging Derived Metrics of the Corpus Callosum in Children With Neurofibromatosis Type I. *American Journal of Roentgenology* 200, 44–49.

Forcet, C., Stein, E., Pays, L., Corset, V., Llambi, F., Tessier-Lavigne, M. and Mehlen, P. (2002). Netrin-1-mediated axon outgrowth requires deleted in colorectal cancer-dependent MAPK activation. *Nature* 417, 443–447.

Goebbels, S., Bormuth, I., Bode, U., Hermanson, O., Schwab, M. H. and Nave, K.-A. (2006). Genetic targeting of principal neurons in neocortex and hippocampus of NEX-Cre mice. *genesis* 44, 611–621.

Gómez-Palacio-Schjetnan, A. and Escobar, M. L. (2008). In vivo BDNF modulation of adult functional and morphological synaptic plasticity at hippocampal mossy fibers. *Neuroscience Letters* 445, 62–67.

Gong, S., Doughty, M., Harbaugh, C. R., Cummins, A., Hatten, M. E., Heintz, N. and Gerfen, C. R. (2007). Targeting Cre Recombinase to Specific Neuron Populations with Bacterial Artificial Chromosome Constructs. *Journal of Neuroscience* 27, 9817–9823.

Goold, R. G. and Gordon-Weeks, P. R. (2005). The MAP kinase pathway is upstream of the activation of GSK3β that enables it to phosphorylate MAP1B and contributes to the stimulation of axon growth. *Molecular and Cellular Neuroscience* 28, 524–534.

Goyal, Y., Jindal, G. A., Pelliccia, J. L., Yamaya, K., Yeung, E., Futran, A. S., Burdine, R. D., Schüpbach, T. and Shvartsman, S. Y. (2017). Divergent effects of intrinsically active MEK variants on developmental Ras signaling. *Nat Genet* 49, 465–469.

Greer, P. L., Hanayama, R., Bloodgood, B. L., Mardinly, A. R., Lipton, D. M., Flavell, S. W., Kim, T.-K., Griffith, E. C., Waldon, Z., Maehr, R., et al. (2010). The Angelman Syndrome Protein Ube3A Regulates Synapse Development by Ubiquitinating Arc. *Cell* 140, 704–716.

Guilding, C., McNair, K., Stone, T. W. and Morris, B. J. (2007). Restored plasticity in a mouse model of neurofibromatosis type 1 via inhibition of hyperactive ERK and CREB:

Restored plasticity in NF1 via ERK inhibition. *European Journal of Neuroscience* 25, 99–105.

Guo, J.-Z., Graves, A. R., Guo, W. W., Zheng, J., Lee, A., Rodríguez-González, J., Li, N., Macklin, J. J., Phillips, J. W., Mensh, B. D., et al. (2015). Cortex commands the performance of skilled movement. *eLife* 4, e10774.

Gutmann, D. H., Parada, L. F., Silva, A. J. and Ratner, N. (2012). Neurofibromatosis Type 1: Modeling CNS Dysfunction. *J. Neurosci.* 32, 14087–14093.

Hart, G. and Balleine, B. W. (2016). Consolidation of Goal-Directed Action Depends on MAPK/ERK Signaling in Rodent Prelimbic Cortex. *J. Neurosci.* 36, 11974–11986.

Hatzivassiliou, G., Song, K., Yen, I., Brandhuber, B. J., Anderson, D. J., Alvarado, R., Ludlam, M. J. C., Stokoe, D., Gloor, S. L., Vigers, G., et al. (2010). RAF inhibitors prime wild-type RAF to activate the MAPK pathway and enhance growth. *Nature* 464, 431–435.

Hilal, N., Chen, Z., Chen, M. H. and Choudhury, S. (2023). RASopathies and cardiac manifestations. *Front Cardiovasc Med* 10, 1176828.

Holter, M. C., Hewitt, L. T., Nishimura, K. J., Knowles, S. J., Bjorklund, G. R., Shah, S., Fry, N. R., Rees, K. P., Gupta, T. A., Daniels, C. W., et al. (2021). Hyperactive MEK1 Signaling in Cortical GABAergic Neurons Promotes Embryonic Parvalbumin Neuron Loss and Defects in Behavioral Inhibition. *Cerebral Cortex* 31, 3064–3081.

Huynh, H., Nguyen, T. T. T., Chow, K.-H. K.-P., Tan, P. H., Soo, K. C. and Tran, E. (2003). Over-expression of the mitogen-activated protein kinase (MAPK) kinase (MEK)-MAPK in hepatocellular carcinoma: Its role in tumor progression and apoptosis. *BMC Gastroenterol* 3, 19.

Ibrahim, A. F. A., Montojo, C. A., Haut, K. M., Karlsgodt, K. H., Hansen, L., Congdon, E., Rosser, T., Bilder, R. M., Silva, A. J. and Bearden, C. E. (2017). Spatial working memory in neurofibromatosis 1: Altered neural activity and functional connectivity. *NeuroImage: Clinical* 15, 801–811.

Ishii, A., Fyffe-Maricich, S. L., Furusho, M., Miller, R. H. and Bansal, R. (2012). ERK1/ERK2 MAPK Signaling is Required to Increase Myelin Thickness Independent of Oligodendrocyte Differentiation and Initiation of Myelination. *Journal of Neuroscience* 32, 8855–8864.

Ishii, A., Furusho, M. and Bansal, R. (2013). Sustained Activation of ERK1/2 MAPK in Oligodendrocytes and Schwann Cells Enhances Myelin Growth and Stimulates Oligodendrocyte Progenitor Expansion. *J. Neurosci.* 33, 175–186.

Ito, Y., Sasaki, Y., Horimoto, M., Wada, S., Tanaka, Y., Kasahara, A., Ueki, T., Hirano, T., Yamamoto, H., Fujimoto, J., et al. (1998). Activation of mitogen-activated protein kinases/extracellular signal-regulated kinases in human hepatocellular carcinoma. *Hepatology* 27, 951–958.

Jeanneteau, F., Deinhardt, K., Miyoshi, G., Bennett, A. M. and Chao, M. V. (2010). The MAP kinase phosphatase MKP-1 regulates BDNF-induced axon branching. *Nat Neurosci* 13, 1373–1379.

Jeffrey, K. L., Camps, M., Rommel, C. and Mackay, C. R. (2007). Targeting dual-specificity phosphatases: manipulating MAP kinase signalling and immune responses. *Nat Rev Drug Discov* 6, 391–403.

Jindal, G. A., Goyal, Y., Burdine, R. D., Rauen, K. A. and Shvartsman, S. Y. (2015). RASopathies: unraveling mechanisms with animal models. *Disease Models & Mechanisms* 8, 1167–1167.

Jover, R., Rodrigo, R., Felipo, V., Insausti, R., Sáez-Valero, J., García-Ayllón, M. S., Suárez, I., Candela, A., Compañ, A., Esteban, A., et al. (2006). Brain edema and inflammatory activation in bile duct ligated rats with diet-induced hyperammonemia: A model of hepatic encephalopathy in cirrhosis. *Hepatology* 43, 1257–1266.

Kalil, K. and Dent, E. W. (2014). Branch management: mechanisms of axon branching in the developing vertebrate CNS. *Nat Rev Neurosci* 15, 7–18.

Kang, M. and Lee, Y.-S. (2019). The impact of RASopathy-associated mutations on CNS development in mice and humans. *Mol Brain* 12, 96.

Kaul, A., Toonen, J. A., Cimino, P. J., Gianino, S. M. and Gutmann, D. H. (2015). Akt- or MEK-mediated mTOR inhibition suppresses Nf1 optic glioma growth. *Neuro-Oncology* 17, 843–853.

Kawai, R., Markman, T., Poddar, R., Ko, R., Fantana, A. L., Dhawale, A. K., Kampff, A. R. and Ölveczky, B. P. (2015). Motor Cortex Is Required for Learning but Not for Executing a Motor Skill. *Neuron* 86, 800–812.

Kim, Y. E. and Baek, S. T. (2019). Neurodevelopmental Aspects of RASopathies. *Mol.Cells* 42, 441–447.

Kim, Y. E., Kim, Y.-S., Lee, H.-E., So, K. H., Choe, Y., Suh, B.-C., Kim, J.-H., Park, S. K., Mathern, G. W., Gleeson, J. G., et al. (2023). Reversibility and developmental neuropathology of linear nevus sebaceous syndrome caused by dysregulation of the RAS pathway. *Cell Rep* 42, 112003.

Klesse, L. J., Meyers, K. A., Marshall, C. J. and Parada, L. F. (1999). Nerve growth factor induces survival and differentiation through two distinct signaling cascades in PC12 cells. *Oncogene* 18, 2055–2068.

Klomp, J. E., Klomp, J. A. and Der, C. J. (2021). The ERK mitogen-activated protein kinase signaling network: the final frontier in RAS signal transduction. *Biochemical Society Transactions* 49, 253–267.

Knowles, S. J., Stafford, A. M., Zaman, T., Angara, K., Williams, M. R., Newbern, J. M. and Vogt, D. (2023a). Distinct hyperactive RAS/MAPK alleles converge on common GABAergic interneuron core programs. *Development* 150, dev201371.

Knowles, S. J., Holter, M. C., Li, G., Bjorklund, G. R., Rees, K. P., Martinez-Fuentes, J. S., Nishimura, K. J., Afshari, A. E., Fry, N., Stafford, A. M., et al. (2023b). *Multifunctional requirements for ERK1/2 signaling in the development of ganglionic eminence derived glia and cortical inhibitory neurons*. elife.

Kozorovitskiy, Y., Saunders, A., Johnson, C. A., Lowell, B. B. and Sabatini, B. L. (2012). Recurrent network activity drives striatal synaptogenesis. *Nature* 485, 646–650.

Krenz, M., Gulick, J., Osinska, H. E., Colbert, M. C., Molkentin, J. D. and Robbins, J. (2008). Role of ERK1/2 signaling in congenital valve malformations in Noonan syndrome. *Proc. Natl. Acad. Sci. U.S.A.* 105, 18930–18935.

Lajiness, J. D., Snider, P., Wang, J., Feng, G.-S., Krenz, M. and Conway, S. J. (2014). SHP-2 deletion in postmigratory neural crest cells results in impaired cardiac sympathetic innervation. *Proc. Natl. Acad. Sci. U.S.A.* 111,.

Langdon, Y., Tandon, P., Paden, E., Duddy, J., Taylor, J. M. and Conlon, F. L. (2012). SHP-2 acts via ROCK to regulate the cardiac actin cytoskeleton. *Development* 139, 948–957.

Lavoie, H., Gagnon, J. and Therrien, M. (2020). ERK signalling: a master regulator of cell behaviour, life and fate. *Nat Rev Mol Cell Biol* 21, 607–632.

Lee, J., Urban-Ciecko, J., Park, E., Zhu, M., Myal, S. E., Margolis, D. J. and Barth, A. L. (2021). FosGFP expression does not capture a sensory learning-related engram in superficial layers of mouse barrel cortex. *Proc. Natl. Acad. Sci. U.S.A.* 118, e2112212118.

Lemmon, M. A. and Schlessinger, J. (2010). Cell Signaling by Receptor Tyrosine Kinases. *Cell* 141, 1117–1134.

Levy, S., Lavzin, M., Benisty, H., Ghanayim, A., Dubin, U., Achvat, S., Brosh, Z., Aeed, F., Mensh, B. D., Schiller, Y., et al. (2020). Cell-Type-Specific Outcome Representation in the Primary Motor Cortex. *Neuron* 107, 954-971.e9.

Li, Y. and Hollis, E. (2021). Basal Forebrain Cholinergic Neurons Selectively Drive Coordinated Motor Learning in Mice. *J. Neurosci.* 41, 10148–10160.

Li, W., Cui, Y., Kushner, S. A., Brown, R. A. M., Jentsch, J. D., Frankland, P. W., Cannon, T. D. and Silva, A. J. (2005). The HMG-CoA Reductase Inhibitor Lovastatin Reverses the Learning and Attention Deficits in a Mouse Model of Neurofibromatosis Type 1. *Current Biology* 15, 1961–1967.

Li, C., Scott, D. A., Hatch, E., Tian, X. and Mansour, S. L. (2007). *Dusp6* ( *Mkp3* ) is a negative feedback regulator of FGF-stimulated ERK signaling during mouse development. *Development* 134, 167–176.

Li, X., Newbern, J. M., Wu, Y., Morgan-Smith, M., Zhong, J., Charron, J. and Snider, W. D. (2012). MEK Is a Key Regulator of Gliogenesis in the Developing Brain. *Neuron* 75, 1035–1050.

Lim, B., Dsilva, C. J., Levario, T. J., Lu, H., Schüpbach, T., Kevrekidis, I. G. and Shvartsman, S. Y. (2015). Dynamics of Inductive ERK Signaling in the Drosophila Embryo. *Current Biology* 25, 1784–1790.

López-Juárez, A., Titus, H. E., Silbak, S. H., Pressler, J. W., Rizvi, T. A., Bogard, M., Bennett, M. R., Ciraolo, G., Williams, M. T., Vorhees, C. V., et al. (2017). Oligodendrocyte Nf1 Controls Aberrant Notch Activation and Regulates Myelin Structure and Behavior. *Cell Reports* 19, 545–557.

Madisen, L., Zwingman, T. A., Sunkin, S. M., Oh, S. W., Zariwala, H. A., Gu, H., Ng, L. L., Palmiter, R. D., Hawrylycz, M. J., Jones, A. R., et al. (2010). A robust and high-throughput Cre reporting and characterization system for the whole mouse brain. *Nat Neurosci* 13, 133–140.

Markus, A., Zhong, J. and Snider, W. D. (2002). Raf and Akt Mediate Distinct Aspects of Sensory Axon Growth. *Neuron* 35, 65–76.

Mayes, D. A., Rizvi, T. A., Titus-Mitchell, H., Oberst, R., Ciraolo, G. M., Vorhees, C. V., Robinson, A. P., Miller, S. D., Cancelas, J. A., Stemmer-Rachamimov, A. O., et al. (2013). Nf1 Loss and Ras Hyperactivation in Oligodendrocytes Induce NOS-Driven Defects in Myelin and Vasculature. *Cell Reports* 4, 1197–1212.

Mebratu, Y. and Tesfaigzi, Y. (2009). How ERK1/2 activation controls cell proliferation and cell death: Is subcellular localization the answer? *Cell Cycle* 8, 1168–1175.

Monje, P., Hernández-Losa, J., Lyons, R. J., Castellone, M. D. and Gutkind, J. S. (2005). Regulation of the transcriptional activity of c-Fos by ERK: A novel role for the prolyl isomerase Pin1. *Journal of Biological Chemistry* 280, 35081–35084.

Morris, E. J., Jha, S., Restaino, C. R., Dayananth, P., Zhu, H., Cooper, A., Carr, D., Deng, Y., Jin, W., Black, S., et al. (2013). Discovery of a Novel ERK Inhibitor with Activity in Models of Acquired Resistance to BRAF and MEK Inhibitors. *Cancer Discovery* 3, 742–750.

Nakamura, T., Gulick, J., Pratt, R. and Robbins, J. (2009). Noonan syndrome is associated with enhanced pERK activity, the repression of which can prevent craniofacial malformations. *Proc. Natl. Acad. Sci. U.S.A.* 106, 15436–15441.

Newbern, J. M., Li, X., Shoemaker, S. E., Zhou, J., Zhong, J., Wu, Y., Bonder, D., Hollenback, S., Coppola, G., Geschwind, D. H., et al. (2011). Specific Functions for ERK/MAPK Signaling during PNS Development. *Neuron* 69, 91–105.

Nikolaienko, O., Eriksen, M. S., Patil, S., Bito, H. and Bramham, C. R. (2017). Stimulus-evoked ERK-dependent phosphorylation of activity-regulated cytoskeleton-associated protein (Arc) regulates its neuronal subcellular localization. *Neuroscience* 360, 68–80.

Nowaczyk, M. J. M., Thompson, B. A., Zeesman, S., Moog, U., Sanchez-Lara, P. A., Magoulas, P. L., Falk, R. E., Hoover-Fong, J. E., Batista, D. A. S., Amudhavalli, S. M., et al. (2014). Deletion of *MAP2K2/MEK2* : a novel mechanism for a RASopathy?: *MAP2K2/MEK2* deletion. *Clin Genet* 85, 138–146.

Osterweil, E. K., Chuang, S.-C., Chubykin, A. A., Sidorov, M., Bianchi, R., Wong, R. K. S. and Bear, M. F. (2013). Lovastatin Corrects Excess Protein Synthesis and Prevents Epileptogenesis in a Mouse Model of Fragile X Syndrome. *Neuron* 77, 243–250.

Otsu, N. (1979). A Threshold Selection Method from Gray-Level Histograms. *IEEE Trans. Syst., Man, Cybern.* 9, 62–66.

Owen, J. P., Bukshpun, P., Pojman, N., Thieu, T., Chen, Q., Lee, J., D'Angelo, D., Glenn, O. A., Hunter, J. V., Berman, J. I., et al. (2018). Brain MR Imaging Findings and Associated

Outcomes in Carriers of the Reciprocal Copy Number Variation at 16p11.2. *Radiology* 286, 217–226.

Ozdinler, P. H. and Macklis, J. D. (2006). IGF-I specifically enhances axon outgrowth of corticospinal motor neurons. *Nat Neurosci* 9, 1371–1381.

Parmar, M. S., Jaumotte, J. D., Zigmond, M. J. and Cavanaugh, J. E. (2015). ERK1, 2, and 5 expression and activation in dopaminergic brain regions during postnatal development. *Int. j. dev. neurosci.* 46, 44–50.

Peters, A. J., Lee, J., Hedrick, N. G., O'Neil, K. and Komiyama, T. (2017). Reorganization of corticospinal output during motor learning. *Nat Neurosci* 20, 1133–1141.

Pintchovski, S. A., Peebles, C. L., Joo Kim, H., Verdin, E. and Finkbeiner, S. (2009). The Serum Response Factor and a Putative Novel Transcription Factor Regulate Expression of the Immediate-Early Gene Arc/Arg3.1 in Neurons. *Journal of Neuroscience* 29, 1525–1537.

Polleux, F. and Snider, W. (2010). Initiating and Growing an Axon. *Cold Spring Harbor Perspectives in Biology* 2, a001925–a001925.

Poulopoulos, A., Murphy, A. J., Ozkan, A., Davis, P., Hatch, J., Kirchner, R. and Macklis, J. D. (2019). Subcellular transcriptomes and proteomes of developing axon projections in the cerebral cortex. *Nature* 565, 356–360.

Rai, B., Naylor, P. E., Siqueiros-Sanchez, M., Wintermark, M., Raman, M. M., Jo, B., Reiss, A. L. and Green, T. (2023). Novel effects of Ras-MAPK pathogenic variants on the developing human brain and their link to gene expression and inhibition abilities. *Transl Psychiatry* 13, 245.

Rao, V. R., Pintchovski, S. A., Chin, J., Peebles, C. L., Mitra, S. and Finkbeiner, S. (2006). AMPA receptors regulate transcription of the plasticity-related immediate-early gene Arc. *Nat Neurosci* 9, 887–895.

Rauen, K. A. (2013). The RASopathies. *Annu Rev Genomics Hum Genet.* 14, 355–369.

Rauen, K. A. (2022). Defining RASopathy. *Disease Models & Mechanisms* 15, dmm049344.

Ray, L. B. and Sturgill, T. W. (1987). Rapid stimulation by insulin of a serine/threonine kinase in 3T3-L1 adipocytes that phosphorylates microtubule-associated protein 2 in vitro. *Proceedings of the National Academy of Sciences* 84, 1502–1506.

Roskoski, R. (2019). Targeting ERK1/2 protein-serine/threonine kinases in human cancers. *Pharmacological Research* 142, 151–168.

Rumbaugh, G., Adams, J. P., Kim, J. H. and Huganir, R. L. (2006). SynGAP regulates synaptic strength and mitogen-activated protein kinases in cultured neurons. *Proc Natl Acad Sci U S A* 103, 4344–4351.

Ryu, H.-H. and Lee, Y.-S. (2016). Cell type-specific roles of RAS-MAPK signaling in learning and memory: Implications in neurodevelopmental disorders. *Neurobiology of Learning and Memory* 135, 13–21.

Santini, C. C., Longden, J., Schoof, E. M., Simpson, C. D., Jeschke, G. R., Creixell, P., Kim, J., Wu, X., Turk, B. E., Rosen, N., et al. (2019). Global view of the RAF-MEK-ERK module and its immediate downstream effectors. *Sci Rep* 9, 10865.

Shaul, Y. D. and Seger, R. (2007). The MEK/ERK cascade: From signaling specificity to diverse functions. *Biochimica et Biophysica Acta (BBA) - Molecular Cell Research* 1773, 1213–1226.

Shigeoka, T., Jung, H., Jung, J., Turner-Bridger, B., Ohk, J., Lin, J. Q., Amieux, P. S. and Holt, C. E. (2016). Dynamic Axonal Translation in Developing and Mature Visual Circuits. *Cell* 166, 181–192.

Steinhoff, J. S., Lass, A. and Schupp, M. (2021). Biological Functions of RBP4 and Its Relevance for Human Diseases. *Front. Physiol.* 12, 659977.

Steward, O. and Worley, P. F. (2001). Selective targeting of newly synthesized Arc mRNA to active synapses requires NMDA receptor activation. *Neuron* 30, 227–240.

Steward, O., Wallace, C. S., Lyford, G. L. and Worley, P. F. (1998). Synaptic activation causes the mRNA for the IEG Arc to localize selectively near activated postsynaptic sites on dendrites. *Neuron* 21, 741–751.

Thomas, G. M. and Huganir, R. L. (2004). MAPK cascade signalling and synaptic plasticity. *Nat Rev Neurosci* 5, 173–183.

Thompson, S. J., Sargsyan, A., Lee, S.-A., Yuen, J. J., Cai, J., Smalling, R., Ghyselinck, N., Mark, M., Blaner, W. S. and Graham, T. E. (2017). Hepatocytes Are the Principal Source of Circulating RBP4 in Mice. *Diabetes* 66, 58–63.

Tidyman, W. E. and Rauen, K. A. (2009). The RASopathies: developmental syndromes of Ras/MAPK pathway dysregulation. *Current Opinion in Genetics & Development* 19, 230–236.

Tiemens, D. K., Kleimeier, L., Leenders, E., Wingbermühle, E., Roelofs, R. L., Sibbles, B., Oostwegel, F. S. M., Vroonland, E., van Leeuwen, C., Niessen, H., et al. (2023). The most important problems and needs of rasopathy patients with a noonan syndrome spectrum disorder. *Orphanet J Rare Dis* 18, 198.

Titus, H. E., López-Juárez, A., Silbak, S. H., Rizvi, T. A., Bogard, M. and Ratner, N. (2017). Oligodendrocyte RasG12V expressed in its endogenous locus disrupts myelin structure through increased MAPK, nitric oxide, and notch signaling. *Glia* 65, 1990–2002.

Tomson, S. N., Schreiner, M. J., Narayan, M., Rosser, T., Enrique, N., Silva, A. J., Allen, G. I., Bookheimer, S. Y. and Bearden, C. E. (2015). Resting state functional MRI reveals abnormal network connectivity in neurofibromatosis 1. *Human Brain Mapping* 36, 4566–4581.

Tsai, W.-H. (1985). Moment-preserving thresolding: A new approach. *Computer Vision, Graphics, and Image Processing* 29, 377–393.

Ünal, E. B., Uhlitz, F. and Blüthgen, N. (2017). A compendium of ERK targets. *FEBS Lett* 591, 2607–2615.

Wang, Y., Kim, E., Wang, X., Novitch, B. G., Yoshikawa, K., Chang, L.-S. and Zhu, Y. (2012). ERK Inhibition Rescues Defects in Fate Specification of Nf1-Deficient Neural Progenitors and Brain Abnormalities. *Cell* 150, 816–830.

Wen, Y., Alshikho, M. J. and Herbert, M. R. (2016). Pathway Network Analyses for Autism Reveal Multisystem Involvement, Major Overlaps with Other Diseases and Convergence upon MAPK and Calcium Signaling. *PLoS ONE* 11, e0153329.

Whishaw, I. Q., Pellis, S. M., Gorny, B., Kolb, B. and Tetzlaff, W. (1993). Proximal and distal impairments in rat forelimb use in reaching follow unilateral pyramidal tract lesions. *Behavioural Brain Research* 56, 59–76.

Wu, X., Simpson, J., Hong, J. H., Kim, K.-H., Thavarajah, N. K., Backx, P. H., Neel, B. G. and Araki, T. (2011). MEK-ERK pathway modulation ameliorates disease phenotypes in a mouse model of Noonan syndrome associated with the Raf1(L613V) mutation. *J Clin Invest* 121, 1009–1025.

Xing, L., Larsen, R. S., Bjorklund, G. R., Li, X., Wu, Y., Philpot, B. D., Snider, W. D. and Newbern, J. M. (2016). Layer specific and general requirements for ERK/MAPK signaling in the developing neocortex. *eLife* 5, e11123.

Ying, S.-W., Futter, M., Rosenblum, K., Webber, M. J., Hunt, S. P., Bliss, T. V. P. and Bramham, C. R. (2002). Brain-Derived Neurotrophic Factor Induces Long-Term Potentiation in Intact Adult Hippocampus: Requirement for ERK Activation Coupled to CREB and Upregulation of *Arc* Synthesis. *J. Neurosci.* 22, 1532–1540.

Yun, M.-S., Kim, S.-E., Jeon, S. H., Lee, J.-S. and Choi, K.-Y. (2005). Both ERK and Wnt/β-catenin pathways are involved in Wnt3a-induced proliferation. *Journal of Cell Science* 118, 313–322.

Zalfa, F., Giorgi, M., Primerano, B., Moro, A., Di Penta, A., Reis, S., Oostra, B. and Bagni, C. (2003). The Fragile X Syndrome Protein FMRP Associates with BC1 RNA and Regulates the Translation of Specific mRNAs at Synapses. *Cell* 112, 317–327.

Zamboni, S. L., Loenneker, T., Boltshauser, E., Martin, E. and Il'yasov, K. A. (2007). Contribution of diffusion tensor MR imaging in detecting cerebral microstructural changes in adults with neurofibromatosis type 1. *AJNR Am J Neuroradiol* 28, 773–776.

Zamorano, C., Fernández-Albert, J., Storm, D. R., Carné, X. and Sindreu, C. (2018). Memory Retrieval Re-Activates Erk1/2 Signaling in the Same Set of CA1 Neurons Recruited During Conditioning. *Neuroscience* 370, 101–111.

Zenker, M., Edouard, T., Blair, J. C. and Cappa, M. (2022). Noonan syndrome: improving recognition and diagnosis. *Arch Dis Child* 107, 1073–1078.

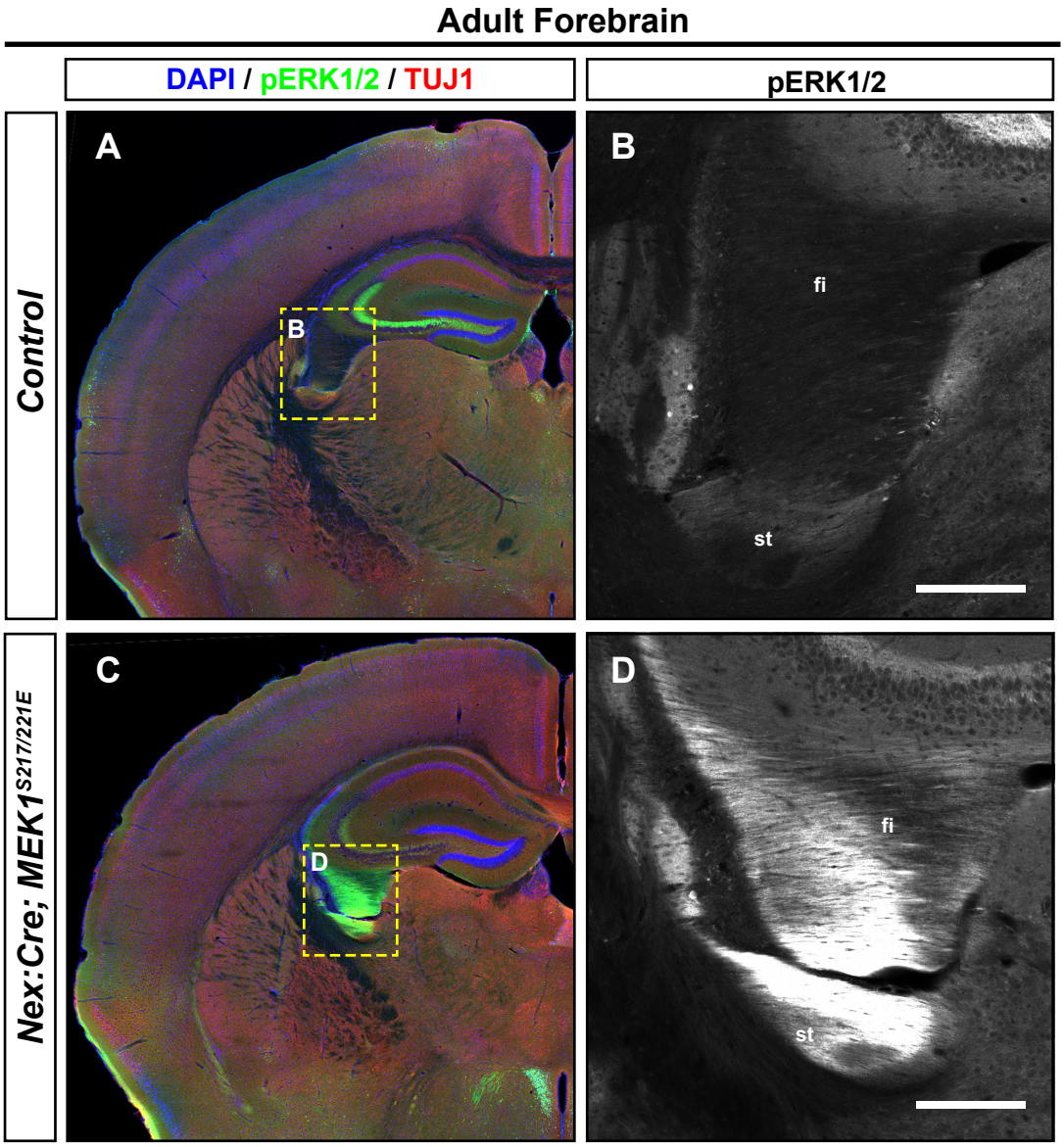
Adult Forebrain
DAPI / pERK1/2 / TUJ1
pERK1/2
Control
Nex:Cre; MEK1S217/221E
A
B
C
D
fi
st

**Supplemental Figure 1. Increased levels of pERK1/2 in hippocampal axons of adult Nex:Cre; MEK1$^{S217/221E}$ mice.**

**A-D.** Immunolabeling of forebrain sections at the level of the adult dorsal hippocampus showed a prominent increase of pERK1/2 within the mutant fimbria and stria terminalis (C-D) relative to controls (A-B), which are enriched in axons derived from excitatory pyramidal neurons in the hippocampal CA1-3 and the amygdala, respectively (n=4, fi = fimbria, st = stria terminalis).

Scale bars = 200μm.

## Adult Forebrain

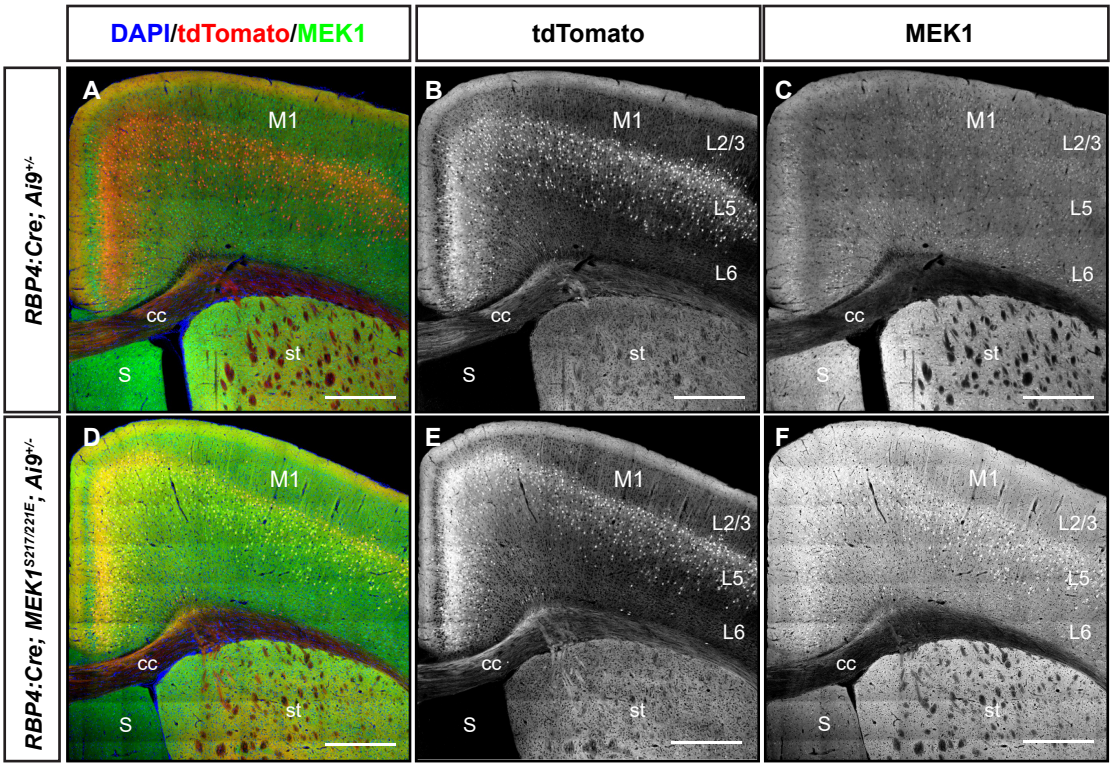


## Adult Spinal Cord

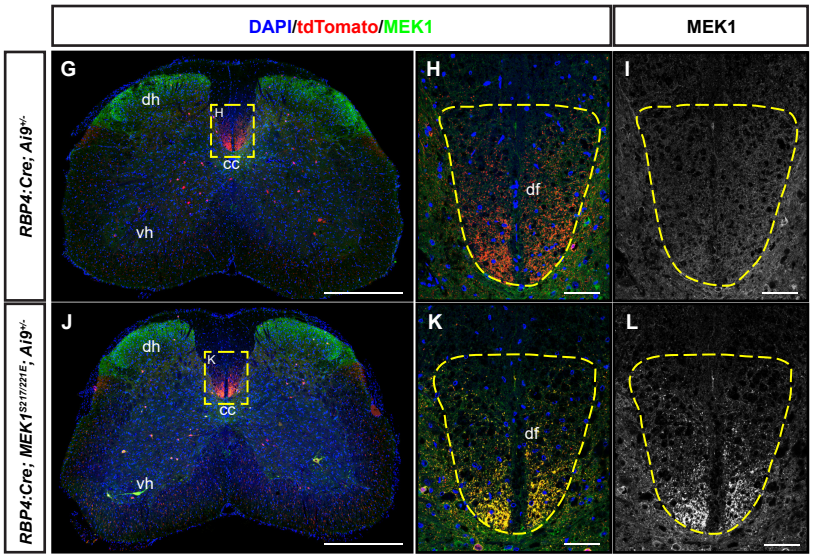


## Adult Liver

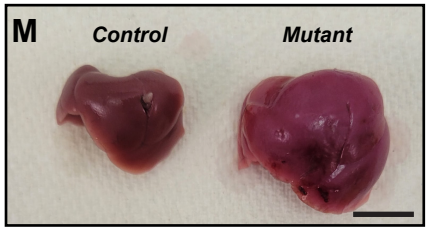

**Supplemental Figure 2. Conditional expression of MEK1$^{S217/221E}$ in RBP4:Cre mice.**

**A-F.** Representative confocal images of *RBP4:Cre; Ai9*$^{+/-}$ cortices. Both *RBP4:Cre; Ai9*$^{+/-}$ mice control and *RBP4:Cre; MEK1*$^{S217/221E}$*; Ai9*$^{+/-}$ mutants express RFP/tdTomato in cortical layer V (A-B, D-E). Immunolabeling of MEK1 showed a robust increase of expression restricted to cortical layer V in mutants (F) compared to controls (C).

**G-L.** Representative images of cross-sectional lumbar segments showing that RFP is detected in descending projections in the dorsal funiculus of controls (G-H) and mutants (J-K). High resolution images reveal increased MEK1 expression in RFP-labeled axons of mutants (K-L) compared to controls (H-I).

**M.** Gross dissection of the mutant liver was suggestive of hepatomegaly when compared to littermate controls (M). (M1 = primary motor cortex, cc = corpus collosum, st = striatum, S = septum, dh = dorsal horn, vh = ventral horn, cc = central canal, df = dorsal funiculus).

Scale bars = Forebrain: A-F = 500 µm, Spinal Cord: G, K = 500µm, H-I, K-L = 50µm, Liver: M = 1cm.

## AAV:*CAG-FLEX-tdTomato* P1 Injection: Collect P30

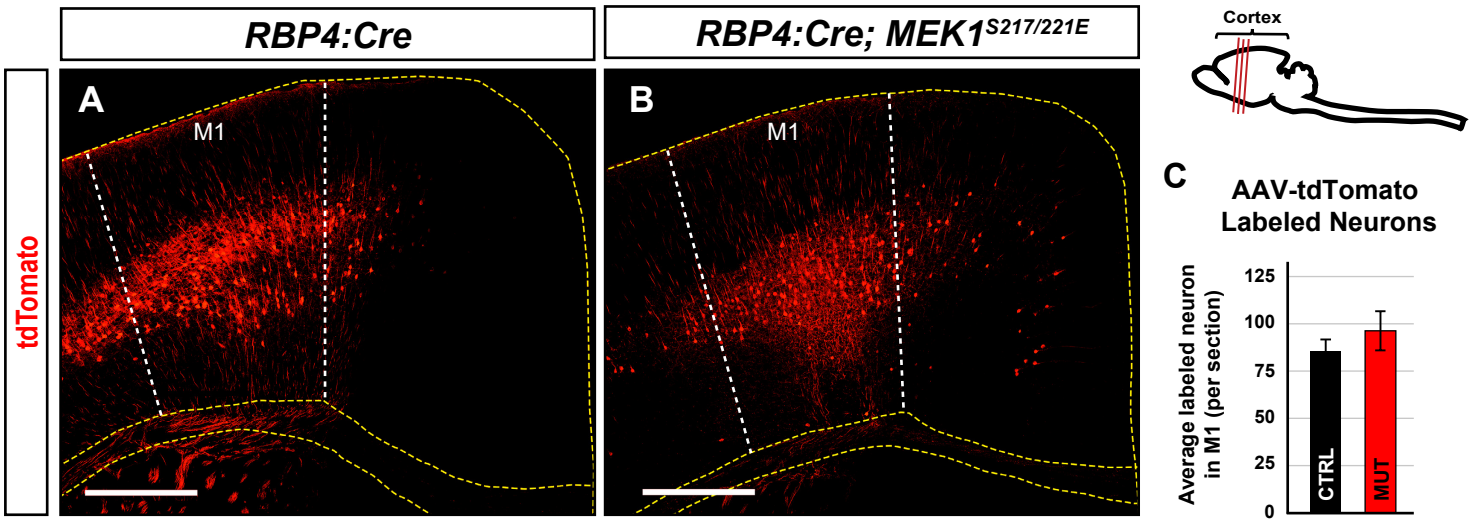


## Corticobulbar Tract Labeling

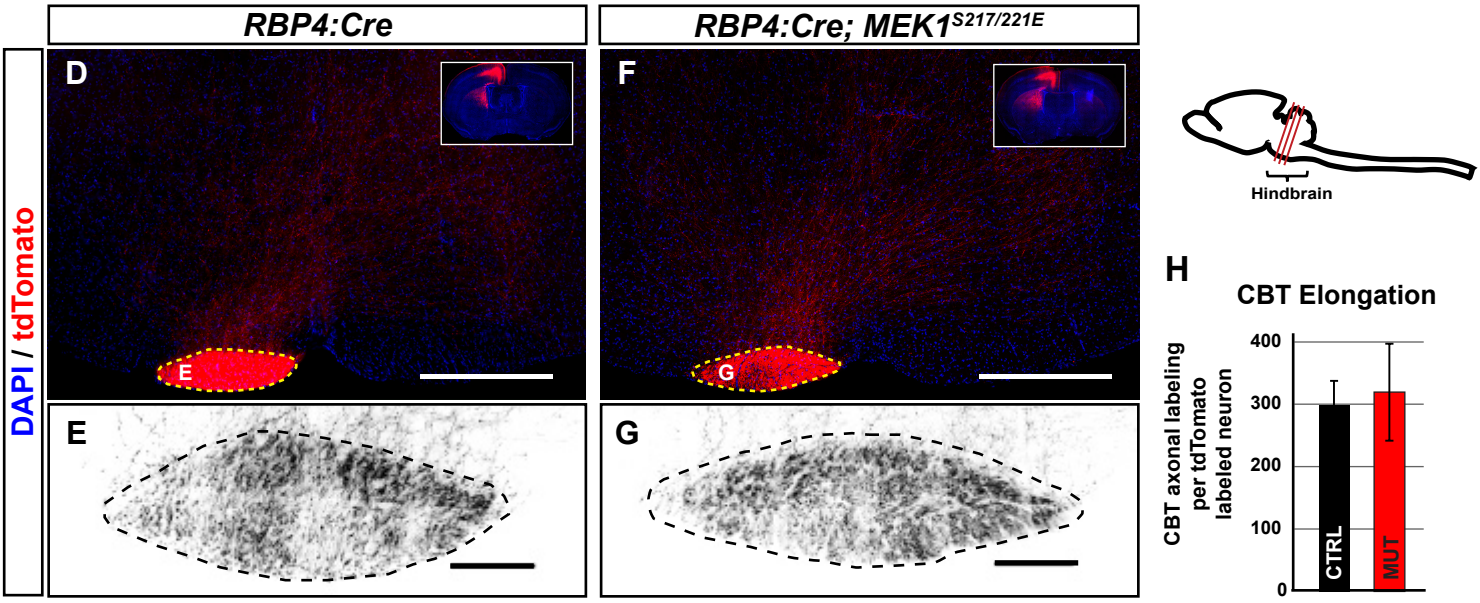

**Supplemental Figure 3. Corticobulbar tract axonal extension is not affected in *RBP4:Cre; MEK1$^{S217/2121E}$* mice.**

**A-C.** Representative AAV injection sites in M1. AAV-tdTomato labeled cell counts in the motor cortex showed no significant differences between *RBP4:Cre;MEK1$^{S217/221E}$* (B) and *RBP4:Cre* (A) mice as quantified in C ($RFP^+$ cells per section, mean ± SEM, n=5, Student's t-test p=0.4). **D-H.** Representative images of corticobulbar tract labeling. Quantification of tdTomato labeled axons in the corticobulbar tract revealed no significant differences between the *RBP4:Cre; MEK1$^{S217/221E}$* (F-G) and *RBP4:Cre* (D-E) control mice (normalized to labeled neurons, mean ± SEM, n=4, Student's t-test, p=0.818) (H).

Scale bars: A,B,D,F = 500μm, E,G= 20μm.

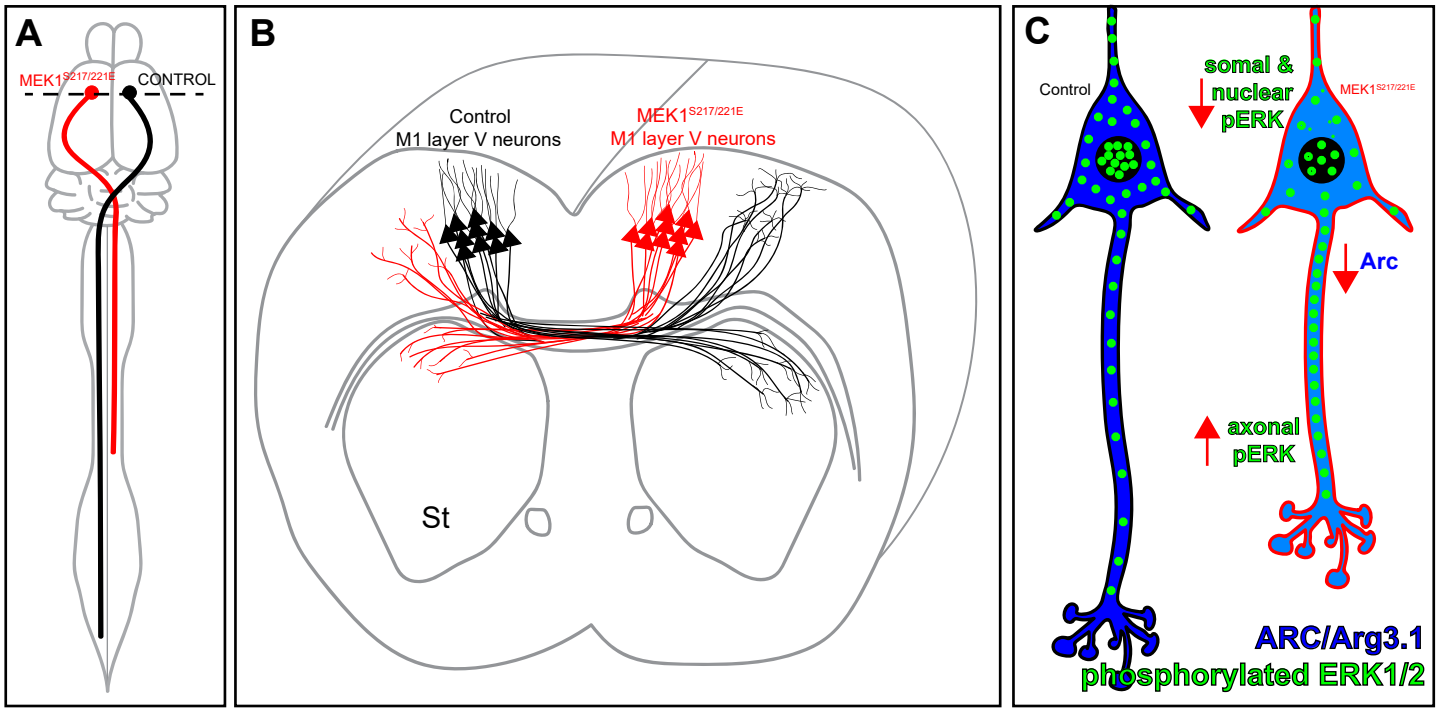
A
MEK1S217/221E
CONTROL
B
Control
M1 layer V neurons
MEK1S217/221E
M1 layer V neurons
St
C
Control
somal &
nuclear
pERK
MEK1S217/221E
Arc
axonal
pERK
ARC/Arg3.1
phosphorylated ERK1/2

**Supplemental Figure 4. Model of aberrant circuit development in excitatory neuron-specific *MEK1*$^{217/221E}$ mice.**

**A-C.** *MEK1*$^{S217/221E}$ expressing layer V neurons (red) exhibit reductions in corticospinal axon elongation along the dorsal funiculus (A), reduced arborization in contralateral cortex and striatum (B), and persistent increases in axonal pERK1/2 (C - green dots) when compared to control neurons (black). These axonal deficits in *Nex:Cre; MEK1*$^{S217/221E}$ mutants coincide with decreased levels of pERK1/2 in the soma and nucleus and reduced expression of activity regulated cytoskeleton-associated protein, ARC (blue), which may underly select deficits in learning a skilled forelimb task (C).